2018

Beach-Ridge Sedimentology as an Archive of Terrestrial Climate Change: Insights From Geochemical and Stratigraphic Study of the Tijucas Strandplain, Southern Brazil

Julie Lauren Krask
College of William and Mary - Virginia Institute of Marine Science, jlkrask@vims.edu

Beach-ridge sedimentology as an archive of terrestrial climate change: Insights from a geochemical and stratigraphic study of the Tijucas Strandplain, southern Brazil

A Thesis

Presented to

The Faculty of the School of Marine Science

The College of William and Mary in Virginia

In Partial Fulfillment

of the Requirements for the Degree of

Master of Science

by

Julie Lauren Krask

August 2018

APPROVAL PAGE

This thesis is submitted in partial fulfillment of

the requirements for the degree of

Master of Science

Julie Lauren Krask

Approved by the Committee, August 2018

Christopher J. Hein, Ph.D.
Committee Chair / Advisor

Valier Galy, Ph.D.

Elizabeth A. Canuel, Ph.D.

James E. Perry, Ph.D.

Steven A. Kuehl, Ph.D

TABLE OF CONTENTS

ACKNOWLEDGEMENTS

There are many people I would like to thank for their support and encouragement over the last several years while I worked towards completing this project. First and foremost, I owe tremendous thanks to my advisor, Chris Hein, for his willingness to take me on as an adopted graduate student from a different field and his nearly endless patience as I tried to make transition, encountering several personal and professional setbacks along the way. He provided constant positivity, never expressed any doubt that I was making progress getting up to speed on new science and was always ready to boost my confidence. A pre-eminent educator and wonderful advisor, I will miss working with him.

In addition, I would like to thank my advisory committee members Dr. Valier Galy, Dr. Elizabeth Canuel, Dr. Jim Perry and Dr. Steve Kuehl, all of whom were invaluable in the development of my project and hypothesis. Their dedication to and excellence in their areas of research is admirable - I am grateful for getting to work closely with them and discuss engaging science.

For abundant technical support over the course of this project, I would particularly like to thank Yanhua Feng and Jenn Connell from VIMS and Carl Johnson and Sean Sylva from WHOI. These individuals were integral to moving lab work forward and obtaining the data necessary for putting together the Tijucas story. Also, I owe Amanda Knobloch so much gratitude for her help with showing me the ropes of organic geochemistry with respect to both lab work and fundamental background information.

Coordinating the logistics of an international project is no easy task, and it certainly could not have been accomplished without the help of multiple collaborators both on US soil and abroad. Thank you to Duncan FitzGerald and Ioannis Georgiou for their mentorship and assistance with fieldwork in Brazil in both 2016 and 2017, and for all the grand times shared over caipirinhas. I have very fond memories of those trips and I learned very much from these individuals. Also, thank you to Antonio Klein, Luis Henrique Polido de Souza and Luis Augusto Santos Madureira for assistance with sample processing and transport across international borders.

One of the most valuable facets of my tenure at VIMS is the friendships I have made and the community I have been a part of. The incoming class of 2015 is a group of folks and a set of memories that will not soon be forgotten. I am grateful for the time I've been able to spend with them. Also to the resident grad students at VIMS that welcomed my fellow classmates and myself at the time, and the lasting relationships that have come as a result of the community bringing each other together. In particular, thanks to esteemed VIMS alums Alison O'Connor, Josh Stone and Randy Jones for being some of the most supportive, encouraging and wise role models anyone could ask for, particularly in times of adversity. As my long-term office mate, Alison truly set the precedent for the best person I could imagine spending my 9-5 next to and the best kind of friend anyone could have. Additionally, I owe a special thank you to Joey Matt for being my running

buddy in the sprint toward the finish, lightening the mood and for building me up when I needed it most.

Most deserving of my gratitude is my family and Bruce Pfirrmann. Thanks to Mom, Dad and Matt for always cheering me on and for their unwavering love and support in whatever I choose to pursue. And finally, thanks to Bruce for being my rock over the last several years. His calming influence, support and patience were unparalleled. I truly could not have seen this through to completion without having him around.

Abstract

Millennial-scale variations in climate forcing are recognized to drive changes in terrestrial processes, and, by extension, impart controls on fluvial sediment loads (*e.g.*, weathering and erosion). However, the impact of decadal- to centennial- scale climate fluctuations on downstream coastal sedimentation patterns and landscape evolution remains unclear. Specifically, the connection between long-term (decades or more) precipitation intensity/seasonality and sediment export from river systems has not been established. This study examines the manner in which sub-millennial-scale fluctuations in precipitation within a river catchment in southern Brazil are recorded in a coastal sedimentary archive. The 5-km wide Tijucas Strandplain formed over the last 5800 years through the rapid reworking of sediment discharged from the Tijucas River in a regime of falling sea level. Within a beach-ridge plain characterized by an overall shift from sand- to mud- dominance (linked to a long-term reduction in wave energy caused by bay shoaling) are nearly 70 distinct transitions between shore-parallel sand- and mud-dominated facies. To assess the potential role of climate forcings (*e.g.*, precipitation patterns) in controlling the delivery of sediment to this coastal system, changes in bulk organic and inorganic characteristics, as well as terrestrial vascular plant wax fatty acid stable hydrogen (δD) and carbon ($\delta^{13}C$) isotopic values, were measured from samples collected across sandy and muddy segments of the plain, and from the modern river, estuary, and bay. Bulk $\delta^{13}C$ measurements from modern system samples increase by 3.3 ‰ from the most upstream sampling location to the estuary, indicating considerable mixing and/or replacement of terrestrial with marine organic material prior to sediment preservation in the strandplain. However, C_{28} fatty-acid $\delta^{13}C$ data indicate that the plain faithfully records the terrestrial component of the organic matter pool. Concurrent and equal magnitude shifts in δD values (tracking precipitation source/amount changes) between 2015 and 2017 of both river and beach sediments indicate that river sediments are rapidly transported from the river-estuary interface, onto the modern beach, and preserved within the strandplain. This interannual variability was absent from bulk and biomarker $\delta^{13}C$ values, reflecting the slower response of vegetation dynamics to precipitation changes. Modern isotopic data from rainfall characterized by seasonally alternating northeast (distal) and southeast (proximal) sources indicates that relatively isotopically depleted average annual rainfall reflects a higher ratio of austral summer to austral winter precipitation, and thus enhanced seasonality. Long-term changes in these precipitation patterns are observed in strandplain biomarker data: δD values become ~10 ‰ more depleted over the last *ca.* 2000 years, reflecting a gradual moistening and/or decreased seasonality of regional climate. This is supported by strandplain biomarker $\delta^{13}C$ values, which record a long-term shift towards more C3-dominated continental vegetation. Moreover, sand-dominated strandplain segments have biomarker δD values indicative of enhanced seasonality (or aridity), as compared with mud-dominated strandplain segments. It is concluded that drier and/or more seasonal rainfall allows for deeper erosion of soils and enhanced export of sand from the Tijucas River, and that changes in the balance of precipitation source and amounts can force substantial changes in the texture and rate of sediment delivery to the coast.

Beach-ridge sedimentology as an archive of terrestrial climate change: Insights from a geochemical and stratigraphic study of the Tijucas Strandplain, southern Brazil

1. Introduction

Most of the global population lives along or near the world's coasts. As such, there has been a growing need for scientific investigation of the impacts of climate change on associated sedimentary coastal systems. However, most work to date has focused on our ability to predict coastal response to projected accelerations in sea-level rise and changes in the frequency or intensity of storms, which are occurring on a global scale. In contrast, there remains a considerable gap in knowledge regarding the interplay between changes in regional and local climate forcings and sedimentation/erosion processes on millennial or shorter time scales. In particular, recent studies have emphasized the importance of understanding how the rate and nature of sediment delivery to the coast by fluvial systems respond to changing climatic and hydrologic regimes, and how this impacts coastal landscape evolution (Blum and Roberts 2009; Hein *et al*. 2011).

Millennial-scale variations in climate forcings drive changes in terrestrial processes that are well documented to be directly linked to fluvial sediment loads (*e.g.*, weathering and erosion) (Bull 1991; Tucker and Singlerland 1997; Whipple 2009). However, the impact of decadal- to centennial- scale climate fluctuations on downstream coastal sedimentation patterns and landscape evolution remains unclear. Specifically, the connection between long-term (decades or more) changes in precipitation amount/seasonality and sediment export from river systems has not been established. This study investigated the role of sub-millennial-scale changes in precipitation patterns,

as geomorphically filtered through river sediment discharge, in driving the rate and nature of sedimentation along the coast. We focus on several specific questions: what are the time scales upon which sediment export from moderate-sized river basins respond to climate change? Are precipitation changes on shorter timescales able to substantially affect basin-scale sediment production and resulting river sediment export fluxes? To what degree can we detect climate-driven changes in the rate or type of sediment delivered to the coast?

To address these questions, we use the sedimentologic record provided by a progradational, clastic strandplain in southern Brazil, the Tijucas Strandplain (Figure 1). This system developed through the deposition of fluvially derived sediments as a series of successive beach ridges and cheniers over a period of nearly 6000 years characterized by slow relative sea-level fall. Organic matter exported and deposited concomitantly with fluvial sediments throughout the period of strandplain progradation records climatic and hydrologic conditions at the time of its deposition. This organic matter can thus be used to produce a record of climate change—and coastal response to those changes—since the mid-Holocene. This study investigated the nature of landscape response to climate change and assesses its coastal imprint over the last 5800 years through the collection of paleo-climate data in the form of stable isotopic compositions of organic matter preserved in sediments across the strandplain, and in comparison to sediments from the modern river and coastal zone.

1.1. Strandplains as recorders of paleoenvironmental change

Clastic coastal and nearshore depositional environments may retain imprints of sub-millennial-scale meteorological and oceanographic changes that occurred over the course of their formation (Cecil *et al.* 2003; Kudrass *et al.* 1998). However, depositional hiatuses and the reworking of sediments in the coastal zone (*e.g.*, during storms) often limit the utility of such systems as recorders of climate-associated variability in fluvial sediment export (Buynevich *et al.* 2007). Thus, identifying coastal settings characterized by uninterrupted deposition of river-derived sediments is critical to ascertain the link between terrestrial climate change, river sediment discharge, and coastal evolution.

Where sediment supply exceeds the availability vertical accommodation space, or where accommodation is being reduced due to relative sea-level fall, new littoral sediment can be reworked and incorporated into progradational beach and foredune ridges. Most often, sediment is delivered to the coastal zone and gradually accrues along the shoreline via wind and wave processes (*i.e.*, alongshore transport) to form shore-parallel foredune and beach ridges, respectively (Scheffers *et al*. 2012; Tamura *et al*. 2018). However, high-intensity wave events can also result in pulsed bursts of sediment delivery to the shoreline that can be distinguished in the internal structure of the ridge (Scheffers *et al*. 2012). Over time, ridges laterally accumulate as new incipient foredunes form and progradation continues, effectively 'stranding' the earlier ridge and preserving the sedimentary record it contains. This process leads to the development of complex coastal landforms comprised of topographic ridges called *strandplains* (Roy *et al*. 1994). Because of the processes by which they form, and their high degree of preservation through the accumulation of successive ridges, strandplains may serve as near-continuous recorders of coastal evolutionary processes and associated allogenic forcings.

If progradation is driven by the delivery and rapid integration of sediment from proximal river systems, strandplains can retain a quasi-continuous record of patterns in fluvial sediment discharge and deposition (Tamura 2012). In this manner, sediment—and its associated geochemical signatures archived within river associated strandplains—can provide critical insight on how upstream climate fluctuations occurring on centennial and decadal scales may impact sediment delivery to the coast.

1.2. Tijucas River and Strandplain, Santa Catarina, Brazil

After the last glaciation, global sea level rose rapidly towards modern elevations. In much of the Southern Hemisphere, it reached an elevation of between 1 and 4 meters above modern mean sea level by between 5500 and 6000 years ago (Isla 1989; Mitrovica and Milne 2002; Milne *et al.* 2005; Angulo *et al.* 2006). This highstand was succeeded by relative sea-level fall at a rate of approximately 0.6 meters/1000 years in response to distal isostatic changes in the land surface, and the global glacio-hydroisostatic redistribution of ocean water (Angulo *et al.* 2006). Within Tijucas Bay, forced shoreline regression associated with falling sea level coupled with the rapid alongshore reworking of sediment discharged from the proximal Tijucas River, and led to the formation of the Tijucas Strandplain over the last ~5800 years (FitzGerald *et al.* 2007; Hein *et al.* 2016). The resulting eastward-facing plain is 5 km in length and is located along an irregular bedrock coast in a semi-enclosed coastal basin (100 km^2) fronted by high-relief bedrock headlands and islands that extend 10-18 km seaward of the modern shoreline (Hein *et al.* 2016).

The Tijucas Strandplain is fed by the Tijucas River, a moderate-sized drainage

system characterized by a 2420 km^2 basin and an average discharge of 40m^3 sec^{-1} (Agencia Nacional da Agua 2000). The floodplain is approximately 130 km^2 and accounts for ~5.5% of the area of the river basin. Upstream, the river is bounded by increasingly higher topography and becomes segmented and narrower. Weathering of Archean- and Proterozoic-aged crystalline bedrock throughout the basin has generated saprolite which is up to tens of meters thick; physical weathering of this saprolite supplies fine-grained sediments as well as sand and fine gravel to the Tijucas River (Basei *et al*.,2001; Caruso,2003). Typical seasonal precipitation patterns correspond to measured suspended sediment concentrations of approximately 70 mg/L (Schettini *et al.* 1996). However, sediment discharges in flood flows have been estimated to be two orders of magnitude higher during periods of increased rainfall due to the high relief of the drainage basin (FitzGerald *et al.* 2007).

Climate within the Tijucas River basin is subtropical and moisture is dominantly sourced from the nearby South Atlantic Convergence Zone (SACZ) over the Southern Atlantic Ocean during austral winter (June, July, August) and from the South America Summer Monsoon (SASM) over the Amazon Basin during austral summer (December, January, February) (Zhou and Lau 1998; Marengo *et al.* 2012). An intensified SASM results in greater austral summer rainfall in Southern Brazil, thereby extending precipitation patterns closer to year-round, rather than seasonally concentrated (Zhou and Lau 1998; Cruz *et al*. 2005; Marengo *et al*. 2012). Prevailing winds are from the northeast, but the passage of moderately strong cold fronts induces southerly winds that dominate the regime (Klein 1997). Average austral winters receive ~25% more precipitation than average austral summers (Orselli 1986).

The landscape of southeastern Brazil is generally characterized by a 100–200 km wide band of lowlands bordering the southern Atlantic Ocean that is abutted by highlands ranging from ~500 to 1200 m in elevation (Behling 1998). Several vegetation types are prevalent across this elevation gradient, all of which are of the C3 variety, with their occurrence in particular regions depending primarily on the length of dry seasons. In Santa Catarina State, *campos* vegetation (*e.g.*, subtropical grasslands) is present in the highlands and overlaps with *Araucaria* moist forests, which occur across southeastern Brazil (Behling 1998, Behling 2003). Both *campos* and *Araucaria* vegetation types are present in regions with a humid climate with little to no dry season (0–3 months) (Ledru *et al.* 1998). Additionally, tropical Atlantic rain forests are predominant in southeastern Brazil, largely occupying the band of lowlands and coastal slopes and reaching their climatic limits in the southern area of Santa Catarina State (Behling 1998; Klein 1978; Por 1992). Areas in southeastern Brazil with abundant Atlantic Rainforest have a climate characterized by high humidity, a dry season of less than two months, annual temperatures between 17° and 24°C and precipitation ranges of 1250–2000 mm/year (Behling 1998; Nimmer 1989).

1.3. Holocene climate change impacts on the Tijucas coast

The Tijucas Strandplain is composed of dozens of shore-parallel, topographically high beach and foredune ridges that mark former shoreline positions during its 5800-year period of growth. Sediment comprising the strandplain changes in composition across the plain, from predominantly coarse sand at the mid-Holocene highstand shoreline to fine mud at the modern beachface. This gradual transition from the growth of a sand-

dominated to mud-dominated plain corresponded to a decrease in the thickness of the strandplain as fluvially-derived muds accumulated in the nearshore and reduced vertical accommodation (Hein *et al.* 2016). This reduced shoreface wave energy and inhibited the deposition of abundant sand along the beach, resulting in a gradual transition across the strandplain from sand-dominated at the oldest, western segments (deposited at the head of a deep bay) to mud-dominated in recent centuries as the bay filled nearly completely with mud. Moreover, this same reduction in accommodation resulted in an increase in progradation rates from ~0.4 meters per year in the early-middle Holocene to close to 3 meters per year in recent centuries as less sediment (and thus less time) was required to laterally grow the plain by a given amount (Hein *et al.* 2016; Figure 2).

Imprinted upon the gradual transition from a sandy to muddy progradational system are 68 distinct shifts between shore-parallel sand- and mud- dominated ridges (Figure 3). Sand-dominated strandplain segments are 3–8 m in thickness and underlain by basin-fill mud; the strandplain unit itself is composed almost entirely of sand in these segments (Hein *et al.* 2016). By contrast, mud-dominated strandplain segments are chenier-like; that is, they are generally composed of alternating thin sandy ridges sitting atop, and laterally separated by, thick muddy units (Figure 4). Individual sand-dominated and mud-dominated strandplain segments are distinguishable in both topography (mud-dominated segments are generally lower in elevation and contain less-distinguishable topographic ridges) and through subsurface imaging (ground-penetrating radar; Figure 4). Moreover, these remain consistently ordered across the 6-km long shoreline (Figure 3).

Despite a progressive decrease in wave energy available to concentrate coarse sediments along the shoreline through time, the strandplain exhibits regular returns from

mud-dominance to sand-dominance, even in the younger, thinner, and overall muddier sections of the plain. This suggests that, unlike the overall shift from sandy to muddy composition over time (reflecting overall reduction in wave energy; Hein *et al.* 2016), the second-order textural composition of the strandplain (semi-regular alternations between sand- and mud- dominance) is controlled by other, allogenic processes. Specifically, we hypothesize that the compositional sedimentary transitions observed across the Tijucas Strandplain reflect sub-millennial changes in sediment delivery to the coast in response to climate-driven variations in drainage-basin sediment production.

1.4. The Tijucas Strandplain: An ideal recorder of coastal response to Holocene climate change

The Tijucas Strandplain grew through the amalgamation of successive sandy beach ridges and mud-dominated cheniers, each set progressively protecting those formed earlier from erosion and reworking by waves. The strandplain also formed within an embayment semi-protected by fronting headlands (Figure 1), thus providing moderate protection from storms which could rework large portions of the plain (*e.g.*, sediments deposited over the prior decades or longer of progradation). This is supported by the clear evidence of a uni-directional decrease in wave energy through the late Holocene (Hein *et al.* 2016), effectively eliminating wave energy as a relevant control on coastal evolution. As such, the Tijucas Strandplain can be considered to provide a near-continuous record of deposition during its nearly 6000-year period of progradation, and the sedimentologic transitions observed within the plain are most likely to reflect changes in the rate and/or texture (grain size) of sediment delivered to the shoreline.

Sediment is delivered to a segment of beach either through cross-shore movement from the shoreface and shallow shelf, or through alongshore movement from an updrift source (*e.g.*, a river mouth). The headlands fronting Tijucas Bay prevent import into the bay of shallow shelf sand moving north within the deeper littoral zone as part of the regional northerly longshore sediment regime (Giannini 1993; Dillenburg *et al*. 2006); this latter observation is supported by the lack of sand and ubiquitous mud throughout Tijucas Bay, as well as the sedimentological disparity between sand composing the strandplain and that transported within the coastal zone outside of Tijucas Bay (Hein *et al.* 2016). Together, these observations suggest that the sediment forming the strandplain is dominantly (or exclusively) derived from the Tijucas River, and is reworked alongshore by relatively low-energy waves within Tijucas Bay. As such, it is assumed that sand-mud transitions across the plain reflect changes in the type or rate of fluvial sediment delivery to the coast, rather than sediment provenance.

A final feature of the Tijucas Strandplain makes it even more ideally suited to record the impacts of sub-millennial-scale climate changes on the coastal zone: the source of sediment to the plain (the Tijucas River) is located in a particularly sensitive climatic zone. Small positional shifts of the Intertropical Convergence Zone (ITCZ) can have amplified effects on precipitation intensity over the region of southeastern South America occupied by the river basin (Zhou and Lau 1998; Cruz *et al.* 2005; Marengo *et al*. 2012). The river is also considerably smaller and overall more likely to exhibit a substantial response to such shorter-duration and lower-magnitude climatic events than larger river basins, such as that of the Mississippi River or the Ganges-Brahmaputra rivers.

Together, these observations suggest that the sand-mud alternations observed across the Tijucas Strandplain record of the effects of climatic changes within the Tijucas River basin on sediment export by the Tijucas River, and, by extension, the role of sub-millennial-scale climate change in driving coastal evolution.

1.5. Thesis objectives

This study investigated the transitions between mud-dominated and sand-dominated segments of the Tijucas Strandplain and links them to Holocene climate change within the Tijucas River basin. It then seeks to assess key factors that regulate landscape response across the coastal zone following short-term climate changes. To accomplish this, we:

1. Characterize the sedimentary record at Tijucas with respect to compositional changes across the strandplain to establish a temporal framework for changes in its textural composition.
2. Use geochemical signatures of organic matter from the modern system and preserved within the strandplain to elucidate variability in hydrologic/climatic conditions over the course of strandplain formation.
3. Determine whether climate forcings have a regulatory role in upstream sediment processes and if they can be linked to sand/mud transitions across the strandplain.

2. Approach and Methods

2.1. Biomarker-based approach to linking climate and sedimentation

Terrestrially-derived organic matter adsorbed to, and concomitantly transported with, fluvial sediments provides an accessible metric for linking climate patterns that paralleled—and may have influenced—the formation of the Tijucas Strandplain. Lipid biosynthesis in vascular plants records stable-isotopic signatures that are governed by myriad climatic conditions including temperature, atmospheric CO_2 levels, relative humidity and moisture source (Craig and Gordon 1965; Farquhar *et al.* 1982; Hayes 2001; Pancost and Boot 2004). The stable-hydrogen isotopic composition (δD) of vascular plant biomarkers changes in response to hydrological conditions and moisture sources at the time of biosynthesis. Similarly, stable carbon isotopic compositions ($\delta^{13}C$) of vascular plant biomarkers can function as a proxy for vegetation patterns by capturing variability in the relative abundance of C3 to C4 plants, which is largely regulated by moisture availability (Street-Perrott *et al.* 1997; Wang *et al.* 2008). Here, we use δD and $\delta^{13}C$ values in long-chain, even-carbon-number fatty acids of vascular plants (C_{24+} FA) to assess changes in precipitation sources and/or amounts as well as changes in continental vegetation dynamics as they are recorded in the Tijucas Strandplain and modern river system.

2.2. Sample collection

Vibracores (thin-walled aluminum tubes, 7.6 cm diameter) were collected in April

of 2015 at six locations throughout the strandplain. These were distributed approximately even distances between the Holocene highstand shoreline and the modern shoreline. Based on a strandplain-wide ground-penetrating radar (GPR) survey (Hein *et al.* 2016), core locations (Table 1; Figure 5a) were selected to represent three different mud-dominated segments of the strandplain and three sand-dominated segments. This sampling design also enabled us to collect samples that were from distinct, sequential time periods throughout the period of evolution of the strandplain; deposition age estimates, which range from 1200 to 4730 years B.P., are derived from the progradation curve (Figure 2; Hein *et al*. 2016). Additional GPR profiles were collected along *ca* 200–250 m long cross-shore segments of the strandplain centered on coring sites. Radar profiles were collected using a 250 MHz antenna associated with Geophysical Survey Systems, Inc. (GSSI) GPR system. These profiles were used to corroborate our classification of the internal structure of each strandplain segment as either sandy or muddy, place our cores in local stratigraphic context, and provide guidance to ensure cores were collected from undisturbed sediments. GPR profiles were post-processed (site-specific data filtering, variable-velocity migration, gain control) using the RadExplorer (Mala, Inc.) software package.

Total vibracore lengths ranged from 2.3 to 5.8 m. All cores were opened, logged (grain size, sorting, interpreted depositional environment), and photographed at the Laboratory of Geological Oceanography at the Universidade do Vale do Itajaí (UNIVALI). Sediment samples ranging from ~150 grams (mud) to ~1200 grams (sand) were collected for geochemical analyses into pre-muffled jars from at least 1.5 m below the ground surface to ensure they were unaffected by surface processes and not

contaminated with modern soil and organic matter. One additional ~150 gram sample was collected in 2016 from the site of core TJV-54. This was done by hand augering to 315 cm below the surface ~ 5 m from the location of vibracore TJV-54. This approach allowed us to re-sample a ~20 cm thick mud unit from within this sandy strandplain which had been observed in, but not collected from, the associated vibracore.

Additional sediment samples were collected to characterize the modern river, estuarine, and beach environments during the years 2012, 2015, 2016, and 2017 (Table 2, Figure 5b). This sampling scheme enabled us to evaluate inter-annual variability in organic geochemical signatures and consider how the composition of organic matter changes across the river-to-beach continuum. Samples are classified by location across these environments into five zones: upper river (1), middle river (2), lower river (3), estuary (4), and beach/bay (5). The approach of sampling the modern system was important for relating chemical records deposited in the intertidal beach and preserved within the strandplain, which have been affected by the input of marine organic matter, to original fluvial signatures.

Samples (~250 g) from the lower intertidal zone of the modern mud-dominated Tijucas Beach were collected in April 2015 and April 2017, in approximately the same location. Caution was used to avoid any organic matter contamination (*e.g.*, sampled using gloves and muffled glassware) and following removal of any living organic matter (bacterial mats) in the surface 1-2 cm. Tijucas River bedload mud was collected in April 2012, April 2015, April 2016, and April 2017 using a ponar grab sampler and subsampled using gloves and muffled glassware. An additional bedload sand sample was collected by hand from 5-10 cm below the surface of a shallow subaqueous sand bar at

the “upper” Tijucas River site in April 2012. We also collected ~250 g sediment samples from both the Tijucas River floodplain (by hand) and floor of Tijucas Bay (ponar grab sampler), both in April 2016.

Finally, in April 2012, 2015, and 2016, Tijucas River suspended sediment samples were obtained for geochemical analyses. This was accomplished by collecting between 25 (2012) and 300 L (2015, 2016) of river water and filtering it through polyethersulfone (PES) membrane filters with a pore size of 0.22 μm. In 2012, surface water was collected using a pre-rinsed bucket at an artificial constriction at the Rua Geral Capim Branco Bridge in Joáia, Santa Catarina, Brazil. In 2015 and 2016, water was collected by boat using a submersible pump held *ca.* 1 m above the river floor along a mid-river transect moving downstream (upstream start: 27°15'45.47"S and 48°39'49.93"W, downstream end: 27°15'52.38"S and 48°39'6.48"W). Specifically, in 2015, 239 L out of 300 L were filtered through 98 membrane filters. In 2016, 214 L out of 300 L collected were filtered through 100 membrane filters. The volume of water filtered in both years was ultimately limited by the quantity of filters available.

All sediment core and modern environment samples collected for geochemical analysis were freeze-dried at the Madureira Lab in the Department of Chemistry at the Federal University of Santa Catarina (UFSC) and shipped to VIMS for later processing. Suspended sediment filters were rinsed with MilliQ water and gently rubbed and scraped to remove sediment. The resulting sediment-laden water was freeze-dried at VIMS and the dry sediment recombined. Total recovered sediment masses were 0.37 g in 2012, 4.5 g in 2015, and 13 g in 2016.

2.3. Bulk analyses

Bulk biogeochemical characteristics were obtained for aliquots of all core and modern-environment samples (19 total). Freeze-dried sediment samples were split using solvent-rinsed tools and aliquots were taken for bulk organic content (total organic carbon [TOC], total nitrogen [TN], carbon and nitrogen isotopes), bulk inorganic content (major and trace element composition), and bulk radiocarbon analyses. The majority (generally > 90%) of samples was set aside for later solvent extraction.

Weight-percent TOC, TN, C/N ratio, and stable isotopic composition of bulk organic carbon ($\delta^{13}C_{TOC}$) and nitrogen ($\delta^{15}N_{TN}$) were determined at the Mass Spectrometry Facility of the Department of Chemistry and Geochemistry at the Woods Hole Oceanographic Institution (WHOI). All analyses were performed in triplicate on an elemental analyzer coupled to a Finnegan Deltaplus isotope ratio mass spectrometer (EA/IRMS). Total and isotopic nitrogen compositions were measured on raw, powdered sample aliquots. Total and isotopic carbon compositions were measured per the protocol of Whiteside *et al.* (2011). Sample aliquots were acidified via fumigation. These were stored in a vacuum desiccator for 60–72 hours at 60–65°C with a beaker containing 50mL of 12N HCL to remove carbonates, after which they were dried for an additional 24 hours in a separate desiccator. Average precision of replicate measurements is 0.26.

Samples used for bulk radiocarbon determination were acidified by HCl fumigation following Whiteside *et al.* (2011) to remove inorganic carbon and then sent to the National Ocean Sciences Accelerator Mass Spectrometry (NOSAMS) facility at WHOI for analysis.

For determination of major and trace element compositions, samples were sent to the Le Service d'Analyse des Roches et des Minéraux (SARM; Centre National de la Recherche Scientifique [CNRS], Nancy, France) where they were analyzed by ICP-AES and ICP-MS following $LiBO_2$ fusion and pre-rinsing (at VIMS) with MillQ to minimize chemical contributions from sea salt.

2.4. Sample preparation for molecular analysis

Lipids for geochemical analyses were extracted from freeze-dried sediment samples for all core and river samples (n=18) with the exception of the 2012 suspended load sample, which did not have sufficient mass for extraction.This was performed using a 9:1 (v:v) dichloromethane:methanol (DCM:MeOH) solvent solution via a microwave-assisted reaction system (MARS, CEMS Corp.) (2012 Tijucas River bedload mud and bedload sand samples) or an Accelerated Solvent Extraction (ASE) system (Dionex ASE 350) (all other samples). The total lipid extract (TLE) for all samples was concentrated by turbovapping and then saponified with a 0.5M KOH in MeOH solution and MilliQ water. The solution was heated in 40 mL vials for 3 hours at 70°C on a flexi-vap workstation heating block, after which 15 mL MilliQ and 0.5 g of NaCl were added and the solution was let cool. Once cool, liquid-liquid extraction was carried out using five, 5 mL hexane rinses to isolate a basic lipid fraction and then the remaining solution was acidified to a pH of 2 via dropwise addition of 12N HCl. Next, five, 5 mL passes of a 4:1 hexane:DCM mixture were put through the sample to extract the acidic lipid fraction. The acidic and basic fractions from each sample were then dried over ~1g combusted $NaSO_4$. Acidic and basic lipid fractions were fractionated into compound classes via column chromatography

separately. One gram of a stationary phase of aminopropyl-functionalized silica gel was added to combusted glass visi-prep columns pre-loaded with glass wool. The lipid fractions were sequentially separated into five fractions using the following solvent mixtures: 4 mL hexane to elute hydrocarbons (F1), 7 mL of 4:1 hexane:DCM to elute ketones/esters (F2), 10 mL of 9:1 DCM:acetone to elute alcohols and other polar lipids (F3), 14 mL of 98:2 DCM:formic acid to elute acids (F4), and 18 mL of 1:1 DCM: MeOH for a final flush column (F5).

The F4 fractions of the basic and acidic lipid extracts from the same original sample were recombined into a F4 "total" fraction to consolidate all fatty acids eluted from the sample. Following recombination of F4 fractions, the fatty acids were dried and then methylated using 15 mL of a 95:5 MeOH:12N HCl solution. The fatty acid-methylation solution was purged of air under nitrogen and heated at 70°C on the heat block for 12 hours. To halt the methylation reaction, 15 mL MilliQ water was added and the solution was allowed to cool. Once at room temperature, another liquid-liquid extraction step was performed (five, 5 mL rinses of 4:1 hexane:DCM) to recover the fatty acid methyl esters (FAMEs), which were then dried over $NaSO_4$. In an additional purification step, the FAMEs were placed on a second aminopropyl-functionalized silica gel column and separated via the following elution scheme: 4mL hexane (F1), 7mL hexane:DCM (F2/FAMEs), and 18 mL of 1:1 DCM:MeOH to flush the column (F3).

The purified total F2 FAMEs fraction was then analyzed for cleanliness and quantified using a gas chromatograph-flame ionization detector (GC-FID). The FAME 37 standard from Supelco was run in between sample injections at different concentrations

to enable the calculation of sample FAME concentrations based on peak areas and response factors.

2.5. Stable isotopic analyses

The $\delta^{13}C$ signature of even-numbered FAMEs (C_{12}-C_{34}) in samples were measured in triplicate at the WHOI Mass Spectrometry Facility on a Finnegan Deltaplus IRMS linked with an HP 6890 GC (GCirMS) by a combustion interface that was operated at 850°C. CO_2 reference gas was injected in several pulses during each run to account for instrument drift over the course of the analytical period. This reference gas had been previously calibrated through running several external standards at various concentrations. Replicate $\delta^{13}C$ measurements of even-numbered long chain (C_{24}-C_{34}) FAMEs $\delta^{13}C$ compositions had an average precision of 0.28. FAMEs $\delta^{13}C$ were mass-balance corrected for the addition of one carbon atom per homolog during methylation by measuring the isotopic signature of the methanol used via a Phthalic acid stock with known $\delta^{13}C$ and stable hydrogen (δD) values.

The δD measurements of long-chain-even-numbered FAMEs (C_{24}-C_{34}) were obtained with a Thermo Scientific DeltaVPlus IRMS linked with an Agilent 6980 GC via a pyrolysis interface (GC-TC) that was operated at 1440°C. Propane was injected at several points before and after analysis during each sample run for use as an internal calibration standard. To account for variability in instrumental fractionation, an external standard mix containing eight FAMES and fatty acid ethyl esters of known δD composition (F8 mixture, A. Schimmelmann, Indiana University) was periodically injected and the reference propane δD value was adjusted accordingly to minimize the

average offset between the known δD values of the F8 compounds and their δD measurements by the instrument. Average precision was 2.1. FAME δD measurements were mass-balance corrected for the addition of three hydrogen atoms per homolog which occurs during methylation.

3. Results

3.1. Ground-penetrating radar

Ground-penetrating radar profiles depict different subsurface structure between sandy strandplain segments and muddy strandplain segments (Figure 6). Sandy strandplain segments are generally composed of tens of centimeters of artificial fill (profiles were collected along roads) overlying repetitive, seaward-dipping (at *ca.* 7–10^{o}) reflections down to 4 meters. Muddy strandplain sections are characterized by a layer of fill (*e.g.*, soil, asphalt) at the surface, overlying a ~50 cm sand layer then two or more meters of mud, gradually transitioning at the base of the beach and shoreface mud into underlying basin-fill mud.

3.2. Bulk organic properties

TOC and TN contents are both highly dependent upon sediment surface area, which is partially a function of grain size. For both strandplain and modern samples, TOC contents by weight percent ranged from 0.030% (sand) to 2.297% (mud) and 0.003% (sand) to 0.326% (mud), respectively. TOC: TN ratios range from 12.3 nearest to the highstand and 8.2 nearest to the modern shoreline (Table 3). TOC:TN ratios for the modern river environment varied widely, ranging from 6.6 to 12.2.

3.3. Bulk radiocarbon

Results from bulk radiocarbon analyses are given in Table 4 All measurements had age errors of < 54 years. The uncalibrated bulk radiocarbon ages of the strandplain segments ranged from 900 ^{14}C years at the seaward-most core location to 4,660 ^{14}C years at the landward-most core location. Uncalibrated bulk radiocarbon ages of modern system samples ranged from 555 to 6100 ^{14}C years.

3.4. Bulk $\delta^{13}C$ and fatty acid $\delta^{13}C$ values

Bulk stable carbon istotope values of strandplain sediments ranged from -23.4‰ to -28.6‰ (average: -25.08‰), and appear to oscillate in value between sandy and muddy strandplain segments over time, such that muddy segments are more enriched than sandy segments (Table 5, Figure 7). Bulk δ^{13}C values of modern samples range from -22.6‰ to -25.8‰ (average: -24.1‰) (Table 5).

All strandplain and modern river samples demonstrate a trend of increased ^{13}C depletion with longer carbon chain lengths (Figure 8). This is consistent with the general classification regime of different organic matter sources: marine organic matter is dominated by lower-chain length fatty acids and is more enriched, while terrestrial material is more depleted and primarily constitutes long chain fatty acids.

Differences in isotopic composition among long-chain homologs in both strandplain sediments and modern river sediments were overall small (Table 6). Further discussion of fatty acid (FA) δ^{13}C compositions focuses on C_{28} FA, which was consistently the most abundant homolog and are representative of all of the long-chain homologs.

$\delta^{13}C$ values of C_{28} FA in strandplain sediments ranged from -29.0‰ to -32.6‰. C_{28} FA $\delta^{13}C$ values become more depleted by ca. 0.9‰ between 2000 and 500 years B.P. (Figure 9). $\delta^{13}C$ for TOC values were on average 7.0‰ more enriched than C_{28} FA (Figure 10).

In samples collected from the modern river environment, $\delta^{13}C$ values of C_{28} FA ranged from -29.1‰ to -32.1‰ (average: -31.2‰) (Table 6). There was minimal interannual variability among bedload, beach, and suspended load samples (Figure 11). The offset between $\delta^{13}C$ values of C_{28} FA and TOC described in strandplain samples also occurs in modern river system samples. Bulk organic matter $\delta^{13}C$ were on average 7.3‰ more enriched than C_{28} FA.

3.5. Major and trace element compositions

Sediment Al/Si ratios are commonly used as proxies for grain size and mobile-to-immobile elemental ratios, *e.g.*, Ca/Si or Fe/Si, is used to assess the extent of chemical weathering. Al/Si ratios range from 0.09 mol/mol (sands) to 0.52 mol/mol (muds) across all strandplain and modern system samples (Table 7). Increased chemical weathering is associated with finer texture (smaller grain size) (Figure 12). The modern system mud samples exhibit some variation in Fe/Si ratios but are collectively distinct from modern and strandplain sand samples, and the strandplain mud Fe/Si ratios all fall within the range of the modern muds. The strandplain mud-in-sand sample is a clear intermediate between the fine and coarse end members but is closer in Fe/Si ratio to the sand samples, indicating an overall coarsening of all sediment deposited within the strandplain during sand-dominated periods.

Ca/Si ratios of sands and muds across the strandplain remain consistent through time, indicating that chemical weathering processes are not strongly implicated in changes in strandplain sediment composition (Table 7, Figure 13). The strandplain sands have Ca/Si ratios ranging from 0.0010 mol/mol to 0.0015 mol/mol, while the strandplain muds have Ca/Si ratios ranging from 0.0250 mol/mol to 0.0406. The strandplain mud-in-sand Ca/Si ratio is a sand-like 0.0055 mol/mol.

3.6. Fatty acid δD values

Due to limited sample masses, δD values could only be obtained for C_{28-32} FA for most samples, and only C_{28} and C_{30} FA for the Tijucas River Suspended Load 2016 and the TJV-51 sandy core samples. No data could be obtained for the TJV-56 sandy core sample due to insufficient sample mass. Similar to $\delta^{13}C$ results, reporting and discussion of δD values focuses on C_{28} FA because it was the most abundant homolog in both strandplain and modern system samples, and because we obtained a near-complete dataset for this homolog.

δD values of FA C_{28} in strandplain sediments ranged from -138.7‰ to -160.3‰ (Table 8, Figure 14). The average of δD values from sandy strandplain segments was -155.1 ‰ while the average of values from muddy segments was -143.1‰. Between ~4750 and 4300 years B.P., FA C_{28} δD values become 11.3‰ more enriched. As a function of deposition age across the strandplain, δD values reach peak enrichment at -138.7‰ around 4300 years B.P. Between ~4300 and 1200 years B.P., δD composition decreases by 21.6‰ to the lowest value of -160.3‰ measured in the strandplain.

δD values for C_{28} FA in samples collected from the modern river system range from -138.7‰ to -156.4‰ (average: -148.0‰) (Table 8). For the years 2012 and 2015, Tijucas Beach, Tijucas River Bedload Mud and Tijucas River Suspended Load all have δD values more depleted than -149.9‰ (2012 average: -153.6‰, 2015 average: -153.1‰) (Figure 15). Between the years 2015 and 2017, all modern system samples become progressively more enriched and peak at -138.7‰. Averaged for years 2015, 2016 and 2017, modern river system δD values are -153.1‰, 143.6‰ and -139.3‰ and indicate a distinct increasing trend through time.

4. Discussion

4.1. Insights into the strandplain geochemical archive based on the modern Tijucas River system

4.1.1. Transformations of organic matter along the modern river-to-beach continuum

Data from the modern Tijucas system reveal that, prior to its burial and incorporation into the strandplain, sediment organic matter undergoes several transformations as it is transported from the lower river, to the estuary, bay, and finally to its depocenter on Tijucas Beach. Quantifying these in the modern system is crucial for understanding how the strandplain may archive the terrestrial system response to climatic forcings.

Organic matter entering rivers is already characterized by constituents from diverse terrestrial sources (*e.g.*, fresh leaf waxes, soil organic matter, rock-derived organic matter; Hedges *et al.* 1986; Drenzek *et al.* 2007; Hilton *et al.* 2011; French *et al.* 2018); added to this is aquatic organic matter from within the river itself (Aufdenkampe *et al.* 2007). For sediment and organic matter discharged from the Tijucas River and reaching Tijucas Beach, the initial terrestrial organic matter signatures are further complicated by the addition of marine organic matter (and possible partial replacement of terrestrial organic matter) during transit from the lower river to the beach (Figure 5b, 16a). TOC $\delta^{13}C$ values for river samples collected furthest inland are up to 3.3 ‰ more depleted than samples collected at the mouth of the river and at the beach. This down-estuary enrichment suggests progressive incorporation and mixing of marine material

with existing terrestrially derived material. Organic carbon derived from marine sources such as water column and benthic primary productivity is characteristically more enriched with respect to $\delta^{13}C$ values (Cloern *et al.* 2002; Bianchi and Canuel 2011). TOC:TN values across the river-beach continuum do not, however, depict a clear spatial trend towards decreasing values with distance downstream and towards the beach depocenter (Figure 5b, 16b), as would be expected through the addition of marine organic matter.

Both terrestrial and aquatic organic matter may also undergo some degree of microbial decomposition or biochemical alteration while transiting the river that could explain the absence of a trend similar to that seen in the TOC $\delta^{13}C$ values (Thornton and McManus 1994; Pruski *et al.* 2015). Rates of organic matter diagenesis and remineralization vary widely across compound classes in ways that can considerably impact bulk organic matter characteristics. For example, environmental conditions such as changing temperatures across seasons can influence microbial community structure and metabolism, thereby affecting the reactivity and degradation rates of different organic compound classes on temporal and spatial scales (Rowe et al. 1975; Klump and Martens 1981). However, given the range and variety of compounds comprising the bulk organic matter pool, the role of these factors is difficult to distinguish. Additionally, physical factors such as sediment and organic matter matrix effects as well as sediment and water column mixing patterns affect degradation rates (Wakeham and Canuel 2006; Kuehl et al. 2016).

Investigation of diagenetic behavior of lipids indicates that while fatty acid degradation is influenced by source, long-chain fatty acids are the most resistant to short-

term remineralization (Canuel and Martens 1996). Thus, environmental signatures are likely to be well-preserved in terrestrially-derived fatty acids throughout the period of transport from uplands, across the estuary, and to the Tijucas Beach. Furthermore, deposition and burial of sediments results in the slowing of processes that can transform organic matter, effectively preserving elemental and isotopic compositions at the time of incorporation into the strandplain (Blair and Aller 2012; Brackley *et al*. 2010).

The clear influence of the addition of marine organic material on the overall composition of sedimentary organic matter delivered to Tijucas Beach reveals a fundamental facet of sediment and organic matter transport in this system: sediments reside within the river-estuary mixing zone long enough to acquire an marine-like signature. This observation is supported by the more depleted bulk $\delta^{13}C$ values for the 2012, 2015 and 2016 Tijucas River Suspended Load samples, which likely reflects a higher proportion of fresher (*e.g.*, recently entered into, and rapidly transported by, the river), terrestrial organic material and less mixing/replacement with the marine pool. In contrast, sediments sampled from the muddy river bedload have TOC isotope signatures more closely matching those from the bay and beach, indicating the addition of marine organic matter starting within the lower river.

While sediments transported within bedload sediments reside at the river-estuary interface long enough to incorporate marine organic material, measurements of δD signatures from the modern system constrain this to a relatively short period of time. For the years 2015, 2016 and 2017, C_{28} FA δD compositions of the Tijucas Beach and Tijucas Bedload samples demonstrate a concurrent, and virtually equal magnitude, shift towards greater enrichment over time, indicating rapid delivery and deposition of river-derived

sediments onto the beach (Figure 15). This suggests that the isotopic signatures of even short-term weather/climate shifts (see section 4.2) are rapidly (sub-annual timescale) transferred to the modern beach. Thus, the strandplain likely rapidly integrates even short-term variability into its progradational record, but this will only be faithfully recorded by terrestrially derived organic matter (biomarkers), as the bulk organic-matter pool is clearly strongly influenced by the addition of marine organic matter during transit.

4.1.2. Long-term organic matter transport and preservation in the strandplain

$\delta^{13}C$ TOC values for sediments from the strandplain also suggest some degree of mixing with marine organic matter and depict an oscillating trend across the strandplain in which sandy strandplain segments are consistently more depleted than muddy segments (Figure 7). This suggests that the transport of sand from the river basin to the beach may occur relatively more rapidly (perhaps in flood-associated pulses), and have less time to accumulate marine organic matter, as compared with muds, which are more susceptible to the addition of marine organic matter during transit. Additionally, samples collected from muddy segments across the strandplain have lower TOC:TN ratios than samples collected from sandy strandplain segments, which is consistent with higher proportions of marine organic material (Figure 17) (Bianchi and Canuel 2011).

This explanation is further supported by bulk radiocarbon analyses. The uncalibrated bulk organic matter radiocarbon ages of the strandplain segments ranged from 4,660 ^{14}C years at the landward-most core to 900 ^{14}C years at the seaward-most core. This trend of younger dates closer to the modern shoreline suggests more recent deposition. Calibration of these ages is complicated by the mixture of terrestrial and

marine matter composing the bulk organic matter; the latter derives carbon at least in part from the marine environment, which has an unknown and time-varying reservoir age. However, comparison between the age of strandplain sample organic matter (in ^{14}C years) and the deposition ages derived from interpolation of a strandplain progradation curve based on uncalibrated ^{14}C ages from the original ^{14}C database (Table 1 of Hein *et al.* 2016) can provide a rudimentary assessment of the "residence time" of the bulk organic matter prior to deposition in the strandplain. A longer residence time reflects storage of organic matter in, for example, soils or river floodplains, resulting in the river discharge of organic matter that is significantly pre-aged at the time of export (Drenzek *et al*. 2009; Galy and Eglinton 2011; Schefuß *et al.* 2016). In the Tijucas Strandplain, this pre-aging would be reflected in bulk organic matter ages greater than associated deposition ages. However, given that these are bulk ages, and thus reflect the average age of all organic matter within the sample, any addition of fresh marine organic matter prior to burial along the shoreline would make these bulk ages significantly younger (closer to deposition age).

We find that all strandplain samples except sandy core TJV-51 fall above a 1:1 line between bulk organic matter ^{14}C ages and deposition ^{14}C age (Figure 18), indicating at least some pre-aging of terrestrial organic matter prior to export by the Tijucas River and deposition in the strandplain. This is consistent with the ages of bulk organic matter from the modern river system (*ca.* 750–4000 ^{14}C years; Table 4). However, for all but one sample (TJV-51), strandplain mud samples are younger (with respect to their deposition age) by ~1000 years as compared to strandplain sand samples. This supports observations from bulk TOC:TN and bulk $\delta^{13}C$ that values that, as compared with sandy

strandplain segments, muddy strandplain samples have generally experienced the addition of more marine organic matter prior to burial.

Nonetheless, despite the influence of marine organic material on the bulk C, N, and ^{13}C and ^{14}C compositions, our data reveal that the terrestrially-derived component of the organic matter pool is faithfully, and rapidly (within sub-decadal, if not shorter, time periods), transferred to, and preserved within, the Tijucas Strandplain. Thus, the organic matter preserved within the strandplain record can be used to track climate changes over sub-centennial or shorter timescales. Furthermore, sand-mud textural changes across the strandplain associated with those paleoclimatic shifts may potentially be used to track basin-scale landscape responses to those climate changes.

4.2. Modern precipitation patterns and time-scales of preservation in the paleohydrological record

The alternating seasonal influence of the SASM (distal, northeast source) and moisture derived from the SACZ (proximal, southeast source) (see section 1.2) exerts a primary control on rainfall amounts and isotopic values across southeast Brazil (Kodama 1993). Summer rainfall is sourced from SASM, which originates in the northwest near the Central American border and travels over the Amazon before reaching southeast Brazil (Cruz *et al*. 2009). This initiates a "rainout effect," (Dansgaard 1964) in which heavier isotopes are preferentially removed from an atmospheric water mass with rainfall as the moisture system travels, resulting in progressively more deuterium-depleted rainfall further away from the source (Vuille *et al*. 2012). As a result, SASM-induced rainfall reaching southeast Brazil has a considerably reduced deuterium composition

(more depleted δD values). Conversely, during the winter, rainfall reaching southeast Brazil is derived directly from the SACZ and is more deuterium-enriched due to shorter distance traveled (Cruz *et al.* 2009; Liu and Battisti 2015) (Figure 19).

These variations are reflected in monthly average precipitation δD values at each Rio Clara (São Paulo) and Puerto Alegre (Rio Grande do Sul), located approximately 450 km northeast and 400 km southwest of Tijucas, respectively. These are the nearest locations to the Tijucas River basin, and the only time period, for which such data are available. Available records (2013–2014 in Rio Clara; 1976–1979 in Puerto Alegre) indicate higher deuterium enrichment of rainfall during austral winter as compared with austral summer (Figure 20) (IAEA/WMO 2018). These trends reflect the seasonal balance between isotopically heavy rainfall in the austral winter months (SACZ source) and isotopically light rainfall in the austral winter months (SASM-derived precipitation). In addition to source, the δD values of rainfall can vary as a function of myriad climate forcings such as El Niño/Southern Oscillation (ENSO), changes in austral insolation, temperatures in the Northern Hemisphere and the position of the ITCZ. In particular, sub-annual shifts in the position of the ITCZ influences SASM rainfall amounts in southern Brazil, and can also contribute to the influx of polar cold fronts that converge with tropical air masses and produce intense rainfall events. Furthermore, ENSO events have been found to correspond with higher volumes of austral summer (SASM-associated) rainfall in southeastern Brazil (McGlone *et al* 1992; Martin *et al.* 1993; Behling 1998), and would thus be likely to shift average annual precipitation δD values towards more depleted values.

Comparison of long-term average monthly trends in rainfall isotopic composition

with our time-series river data reveals the means by which interannual changes in precipitation source/amount may be reflected in river-basin fatty acid deuterium values. Total annual precipitation data from 2012-2017 for Florianópolis, SC (~60 km south of Tijucas) indicate that precipitation was highest in 2015 (2291 mm of total rainfall), as compared with only 1462–1602 mm for all other years (Figure 21) (Instituto Nacional de Meterorólogia 2018). Moreover, subdividing these data into rainfall totals over 3-month periods of summer (Nov, Dec, Jan) and winter (Jun, Jul, Aug), as well as 6-month periods of representing extended summer (Nov-Mar) and winter (Apr-Oct) (Figure 22), demonstrates that these annual precipitation totals are highly sensitive to seasonal variability. In particular, the marked increase in total annual precipitation that occurred in 2015 is directly related to rainfall during the extended (6-month) preceding winter precipitation period; in fact, whereas six-month summer and winter rainfall amounts are generally similar (600-900 mm), in 2015 winter precipitation was 544 mm greater than that during the preceding summer period. Given that this winter precipitation is generally locally sourced, and therefore dominated by isotopically enriched water (Figure 19), it is anticipated that the overall rainfall in 2015 would have been significantly more deuterium enriched as compared with other years.

Given that modern system samples from 2015 were collected in April, prior to austral winter, it is expected that δD values from that year would be more depleted than those from 2016 and 2017, following the period of heavy austral winter rainfall. The marked increase in river and beach δD values by *ca.* 8.8‰ between 2015 and 2016 suggests that the signal from the elevated austral winter rainfall in 2015, which is sourced from the SACZ and is more enriched, becomes incorporated into the river system rapidly,

over several months to a year. This year-to-year shift is apparent in all samples, but largest (11 ‰) in the river suspended load. This is as anticipated given that the suspended load is expected to convey the freshest (youngest; e.g., Galy *et al*. 2008) organic matter with a short residence time in the river as compared with bedload sediments. Unfortunately, no such suspended load data are available for 2017. However, δD values of all modern system samples continue to increase between 2016 and this final sampling year. This continued, simultaneous enrichment of organic matter δD signatures of both Tijucas Beach and Tijucas Bedload samples into 2017 is consistent with a sub-annual period of sediment transport across the five river-estuary-beach zones (see section 4.1).

In contrast to our biomarker δD values, which appear to show clear sensitivity to interannual climate, we observe a lack of interannual variability in modern-system C_{28} FA $\delta^{13}C$ values. This indicates that, whereas shorter-term changes in precipitation source appear to be occurring, they are not sufficiently strong to drive basin-wide changes in vegetation dynamics.

4.3. Mechanism underlying paleovegetation and paleohydrological patterns preserved in the strandplain

This study provides insights into the mechanisms by which climate (hydrology) is recorded in organic matter exported by the Tijucas River (section 4.2) and how that organic matter transforms as it moves from the lower river, across the estuary, and to the Tijucas Beach (section 4.1). These allow for application of the paleo-vegetation (bulk and compound-specific fatty acid $\delta^{13}C$ values) and paleo-hydrology (compound-specific fatty acid δD values) proxies recorded within the strandplain for reconstruction of

changes in each basin-wide climate and, in combination with mapping of sand-mud transitions across the plain (Figure 3), the impact of these changes on landscape dynamics.

C_{28} FA $\delta^{13}C$ values of samples collected across the Tijucas Strandplain are generally very depleted (-31.1 to -32.5 ‰) throughout the strandplain record, but become more so through time, particularly over the last ~3000 years. The former is unsurprising given the composition of Tijucas Basin vegetation, which is primarily C3-dominated Atlantic pluvial forest (Behling 1995). However, the latter suggests some response of the basin vegetation community to climate shifts. For example, the enhanced ^{13}C depletion of fatty acids towards the latter part of the record may be reflective of differential fractionation across C3 plant types, which presumably underwent changes in relative abundance throughout the river basin in response to the subtle changes in climate (Kohn 2010). Alternatively, this trend may reflect an overall, gradual, and slight, shift over millennia toward more C3-like signatures (*e.g.*, less overall plant stress), perhaps in response to wetter or less seasonally water-stressed conditions. Either scenario is consistent with other records that demonstrate a gradual transition from relatively dry climate to a wetter climate in southern Brazil around 4000 years B.P. through an increased abundance of grassland (*campos*) vegetation followed by predominance of *Aracauria* forest over the last ~1000 years, as recorded by changes in pollen compositions in sediment cores (Behling *et al*. 2001; Behling *et al*. 2005). Given that the occurrence of these forms of vegetation requires a virtually absent dry season (0-3 months), such records align with reduced plant stress associated with precipitation seasonality (Ledru *et al.* 1998).

In contrast, C_{28} FA δD compositions from across the Tijucas Strandplain show an opposite, but more subtle trend. Values shift from *ca.* -145 ‰ (average of oldest sand and mud strandplain samples) to *ca.* -155 ‰ (average of youngest sand and mud strandplain samples); C_{28} FA δD compositions of mud samples become more depleted by only ~5 ‰ over time. The long-term trend is of similar magnitude to (~10 ‰), though in the opposite direction of, that seen between modern river samples collected following the relatively dry 2011 and 2014 winter rainfall seasons (April 2012 and 2015 samples), and the relatively wet 2015 season (April 2016 and 2017 samples). This appears to suggest that strandplain C_{28} FA δD compositions reflect a gradual aridification (or at least, lessening of the relative role of austral winter [SACZ] rainfall) during the late Holocene. However, such an interpretation is in contrast with our C_{28} FA $\delta^{13}C$ record, which, if anything, suggests climate became wetter, or less seasonal (in response to increased winter precipitation) during the late Holocene.

The apparent discrepancy between our long-term paleo-vegetation and paleo-hydrological records may be explained by the two simply responding to forcings over different timescales. In particular, vegetation dynamics (and thus strandplain-derived river basin $\delta^{13}C$ values) are more likely to represent an integrated, long-term response of the basin to climate forcings. In contrast, δD measurements are more representative of short-term changes in climate, as clearly demonstrated by modern river data (section 4.2). They therefore may represent centennial or shorter variability in the hydrological system clearly evident during the Holocene (Novello *et al.* 2018; Vuille *et al.* 2012). This latter observation may also explain why the long-term decrease in δD values observed across the strandplain is also in contrast to independent proxy records (*e.g.*, Cruz *et al.* 2005),

which generally show a decrease in SASM (and thus austral *summer* precipitation) during the middle to late Holocene. That is, our (spatially and temporally) widely spaced strandplain δD record may simply be responding to short-term (sub-decadal) variability in, *e.g.*, ENSO strength or long-term ITCZ position, as opposed to the long-term trend.

These same shorter-term shifts (or some intermediate centennial-scale climatic variability) may also be reflected in differences between sand- and mud- dominated sections of the strandplain (Figure 14). Muds deposited at ~3000 and ~4500 years B.P. are considerably more deuterium-enriched (by an average of ~16 ‰) than both sand samples (~2000 and ~4700 years B.P.). The mud sample deposited at ~1200 years B.P. has an intermediate δD value. These differences are much less pronounced in $\delta^{13}C$, where C_{28} FA from sand-dominated strandplain segments are, at most, < 1 ‰ more enriched than those from mud-dominated segments.

Nonetheless, biomarker δD values from sand and mud sections tell a consistent story: sandy periods likely correspond to either (1) less austral winter rainfall, and thus drier overall climate, assuming summer SASM precipitation remains unchanged; or (2) less austral winter rainfall and more summer SASM precipitation, and thus more seasonal rainfall. This is supported by the very weak correspondence of sand-dominance with more ^{13}C-enriched (less C3-like) organic matter, suggesting the possibility that those periods correspond to stretches characterized by more water stress (drier, or more seasonal rainfall). Moreover, bulk $\delta^{13}C$ and ^{14}C data all indicate that, under these drier/more seasonal conditions, sediment (dominated by sand) is discharged from the river onto the beach quickly. Conversely, periods of mud dominance during strandplain formation correspond to stretches of wetter conditions, which occur when winter rainfall

extends into months outside of austral winter and becomes more year-round, or less seasonal.

Periods of river sediment discharge characterized by sand versus mud dominance may be explained by the effect of precipitation seasonality on the availability of different sediment types for export from the river. Overall, drier or more seasonal conditions may correspond to deceleration of chemical weathering and soil production throughout the river catchment, resulting in decreased overall amounts of fine sediment available for export. Additionally, drier conditions over the course of the year inherently lead to reduced overall transport capacity and discharges, further reducing overall mud export. Therefore, it is likely that sand-dominated strandplain segments will largely be composed of sediments rapidly mobilized as a result of deep erosion of upper basin hillslopes during flashy, seasonal discharge (perhaps coupled with storm-induced landslides) and only a smaller amount of finer, fresh topsoil sediments eroded from the surface. A similar process has been found to be operating within the Waipaoa River System (New Zealand), in which landsliding associated with periods of intense rainfall produces large volumes of coarse sediment later transported to the coast(Kuehl et al. 2016). Alternatively, periods of extended winter rainfall promote prolonged surface erosion nearly year-round that gradually erodes and removes from the basin fresh vegetation, finer surface sediments, and soil, the latter containing relatively old organic matter. Thus, mud-rich soils from the riverbanks and muddy riverbed are remobilized and gradually move through the river-estuary mixing zone to soon be exported to the beach.

4.4 Alternative interpretations and mechanisms

While data collected from this study most closely align with the explanation of precipitation seasonality exerting a primary control on river sediment export from the river, and therefore textural composition of the strandplain, alternative hypotheses are plausible. For example, our modern data reveal that organic-matter δD signatures from the Tijucas Basin are particularly sensitive to moisture source, as opposed to precipitation amount. Changing the relative proportion of precipitation from each the SACZ and SASM sources would itself alter the annual average precipitation deuterium composition, and thus, organic matter δD signatures. It is therefore possible that our strandplain record of precipitation variability reflects any one of several moisture-source dynamics: the more deuterium-depleted fatty acids associated with sand deposition could reflect increased more SASM-derived rainfall (wetter overall climate), less SACZ-derived rainfall (driver overall climate), or some combination of both (more seasonal climate) during these periods. This complicates our interpretation of the mechanism, and leaves uncertainties given available data.

Furthermore, the interpretation of the apparent interannual variability in δD to reflect a roughly annual scale "lag time" between organic matter synthesis, transport and final deposition in the strandplain is contingent on the assumption that the terrestrial fatty acid pool within the organic material is dominated by fatty acids synthesized in the year prior to sampling. That is, there is an implicit assumption that the C_{28} FA δD signatures are representative of the precipitation patterns over that immediate time period. However, an alternative explanation for the data is that changes in precipitation patterns result in differential erosion processes: elevated 2015 rainfall drove deeper soil erosion, thereby

contributing pre-aged “background” organic matter with a more enriched deuterium signature. In this case, there was likely a longer (multi-year or decadal) period of wetter climate and/or elevated SACZ-derived precipitation over which deuterium-enriched organic matter continued to accumulate in the soils. This is not contradictory to our conclusion regarding the control of precipitation seasonality on sand/mud transitions across the strandplain.

Finally, our proven relationship between climate-controlled terrestrial organic matter isotopic signatures and strandplain texture composition does not preclude secondary impacts on strandplain composition from coastal processes. In particular, decadal- to centennial-scale changes in wind and wave regimes, possibly induced by fluctuating storm climate, cannot be completely ruled out. High quantities of sediment delivered from the Tijucas River have largely driven bay infilling at Tijucas during the period of strandplain growth (see section 1.3). Numerical models demonstrate that this process contributed to a gradual reduction in wave energy during this 5500 year time period (Hein *et al.* 2016). Progressively reduced wave energy is consistent with the transition of the Tijucas Strandplain from sand- to mud-dominated; however, it is possible that the continued return of sandy ridge formation simultaneously suggests the periodic return of relatively stronger waves, or centennial-scale periods of enhanced storminess. For example, Nardin and Fagherazzi (2018) demonstrate through numerical modeling that enhanced storminess can result in a period of erosion of a mud-dominated beach, and therefore temporarily slow progradation and steepen the nearshore. This results in increased concentration of sandy sediments onshore due to elevated wave power. This outcome is unsurprising and consistent with the findings of, for example,

Bever *et al.* (2011) for Poverty Bay, New Zealand. Here, enhanced wave energy reworks results Waipaoa River derived sediments in the nearshore, resulting in the export of fine silts and clays to the shelf and concentration of sands along the prograding shoreline.

Although the mechanism is entirely feasible, no clear correlation between wave energy and strandplain texture can be derived from available data at Tijucas. This in part reflects the dearth of records of Holocene changes in overall wave climate in this part of the Atlantic Ocean. However, a record of ITCZ migration produced based on metal records in the Cariaco Basin off the coast of Venezuela indicates a general downward shift over the course of the Holocene, which could drive changes in storm and wave climate (Haug *et al*. 2001). Furthermore, storm reconstructions from elsewhere in the southern hemisphere may provide insight on the potential for time-varying wave and storm climate in central Santa Catarina. For example, Page *et al.* (2010) developed a record of storm events preserved in lake sediments on North Island in New Zealand and found that episodic increases in major storm activity occurred on centennial scales (~150-350 years) and attributed such changes to the interplay between many of the same climate systems that govern conditions at Tijucas, such as fluctuations in ENSO. Thus, it is probable that storm and wave climate in the Southern Atlantic Ocean has changed over time as a function of ENSO and other major climate systems. Future work at Tijucas will include further refinement of the numerical SWAN models used by Hein et al. (2016) to explore bay infilling processes. These will be used to test how changing boundary conditions (open ocean wave climate) may affect wave energy and the ability to preferentially concentrate sand and mud at the Tijucas coast through the late Holocene, as infilling progressed. This approach will allow us to explore possible secondary

contributions of allogenic coastal processes to the development of the sand-mud transitions observed Tijucas.

5. Conclusions and Future Directions

This work establishes a link between climate patterns and coastal sedimentation on several time scales through a novel approach using combined sedimentological and organic geochemical techniques. In this first-of-its-kind study, we find that a progradational beach- and foredune- ridge plain (the Tijucas Strandplain) can serve as a viable, sub-millennial-scale recorder of changes in precipitation and vegetation dynamics, as filtered through river sediment transport and deposition along the shoreline. Specifically, our results lead us to conclude that precipitation changes are archived within terrestrial organic matter preserved within the strandplain on decadal to centennial scales, whereas subtle changes in vegetation associated with climate fluctuations become integrated over longer time scales and are more readily detectable across millennia. Analysis of the modern river system was critical for confirming the ability of the strandplain to faithfully record isotopic signatures of terrestrially derived organic matter despite considerable integration with marine organic matter pools during transport throughout the river system.

Additionally, our results may point to an alternative (or secondary) mechanism for strandplain-wide changes in sediment texture. Until now, the unidirectional shift in strandplain composition from sand-dominated to mud-dominated has been largely attributed to reduced accommodation and wave energy associated with bay infilling process (Section 1.3; Hein *et al.* 2016). However, the late Holocene shift towards wetter conditions associated with mud-dominated export recorded within the strandplain itself

indicates that sediment erosion and export processes associated with a gradually changing climate may have also played a role. In particular, the enhanced mud export (as compared with sand) may have accelerated bay infilling, thus contributing indirectly to the transition to mud-dominance associated with decreasing accommodation. It may also have allowed for increased delivery of mud directly to the plain, providing a direct forcing of this long-term textural change observed across the plain.

Finally, stable-hydrogen isotopic data most strongly suggest that the balance between SASM-derived rainfall during austral summer and SACZ-derived rainfall during austral winter controls precipitation seasonality, which in turn regulates the type (sand vs mud) and rate of sediment discharged from the Tijucas River, deposited on the beach, and incorporated into the strandplain. However, available data are insufficient to address the nature of the underlying mechanism. Future compound-specific radiocarbon analyses of terrestrial organic matter archived in strandplain and modern river sediments will allow for testing of the hypothesis that relatively subtle, basin-scale changes in precipitation seasonality can sufficiently alter soil erosion processes and river sediment loads such that coastal progradation can switch between sand- and mud- dominated. We hypothesize that precipitation seasonality causes hillslope destabilization and enhanced landsliding, exposing deeper, sandier sediments and associated pre-aged organic matter to physical erosion and river export to the coast. Compound-specific radiocarbon data from isolated terrestrial biomarkers from the modern river and across the strandplain will allow for the determination of the degree of pre-aging of organic matter prior to export, and therefore provenance of sediment and organic matter from within basin soil profiles. This will allow for direct testing of the proposed mechanistic link between climate change, soil

erosion, and coastal sedimentation (Section 4.3).

References

Agencia Nacional da A gua (2000) Estado de Santa Catarina. Available at: hidroweb.ana.gov.br/cd3/sc.doc (accessed 18 October 2010).

Angulo, R. J., Lessa, G. C., and Filho Souza, M. C. d. 2006. A critical review of mid- to late-Holocene sea-level fluctuations on the eastern Brazilian coastline. *Quatern. Sci. Rev.* 25: 486-506.

Aufdenkampe, A. K., Mayorga, E., Hedges, J. I., Llerena, C., Quay, P. D., Gudeman, J., Krusche, A. V. and Richey, J. E. 2007. Organic matter in the Peruvian headwaters of the Amazon: Compositional evolution from the Andes to the lowland Amazon mainstem. *Org. Geochem.* 38: 337–364.

Basei, M.A.S., Campos Neto, M.C., Castro, N.A., Nutman, A.P., Wemmer, K., Yamamoto, M.T., Hueck, M., Osako, L., Siga, O. and Passarelli, C.R. (2001) Tectonic evolution of the Brusque Group, Dom Feliciano belt, Santa Catarina, Southern Brazil. J. S. Am. Earth Sci., 32, 324–350.

Behling, H. 1995.Investigations into the late Pleistocene and Holocene history of vegetation and climate in Santa Catarina (S Brazil). *Vegetation History and Archaeobotany*, 4: 127–152.

Behling, H. 1998. Late Quaternary vegetational and climatic changes in Brazil. *Review of Palaeobotany and Palynology.* 99(2): 143-156.

Behling, H. Bauermann, S.G. and Cesar, P. 2001. Holocene environmental changes in the São Francisco de Paula region, southern Brazil. *Journal of South American Earth Science*. 14(6): 631-639.

Behling, H. Pillar, V. P. and Bauermann, S.G. 2005. Late Quaternary grassland (Campos), gallery forest, fire and climate dynamics, studied by pollen, charcoal and multivariate analysis of the São Francisco de Assis core in western Rio Grande do Sul (southern Brazil). *Review of Palaeobotany and Palynology.* 133(3-4): 235-248

Bever, A. J., McNinch, J. E. and Harris, C. K. 2011. Hydrodynamics and sediment-transport in the nearshore of Poverty Bay, New Zealand: observations of nearshore sediment segregation and oceanic storms. *Cont. Shelf Res.* 31(6): 507-526.

Bianchi, T. S. and Canuel, E. A. 2011. Chemical Biomarkers in Aquatic Systems. Princeton University Press, Princeton, NJ.

Blair, N. E. and Aller, R. C. 2012. The fate of terrestrial organic carbon in the marine environment. *Annu. Rev. Mar. Sci.* 4:401-423.

Blaauw, M. 2010. Methods and code for 'classical' age-modeling of radiocarbon sequences. *Quaternary Geochronology*. 5(5): 512-518.

Blum, M. D. and Roberts, H. H. 2009. Drowning of the Mississippi Delta due to insufficient sediment supply and global sea-level rise. *Nature Geoscience*. 2: 488-491.

Brackley, H. L., Blair, N. E., Trustrum, N. A.., Carter, L., Leithold, E. L., Canuel, E. A., Johnston, J. H. and Tate, K. R. 2010. Dispersal and transformation of organic carbon across an episodic, high sediment discharge continental margin, Waipaoa Sedimentary System, New Zealand. *Marine Geology.* 270(1-4): 202-212.

Bull, W. B. 1991. Geomorphic responses to climate change. Oxford University Press, New York, NY.

Buynevich, I. V., FitzGerald, D. M. and Goble, R. J. 2007. An increase in North Atlantic storm activity over the past 500 years: evidence from optically dated relict beach scarps. *Geology*. 35: 543-546.

Canuel, E. A. and Martens, C. S. 1996. Reactivity of recently deposited organic matter: Degradation of lipid compounds near the sediment-water interface. *Geochimica et Cosmochimica Acta*. 60(10): 1793-1806.

Caruso, F., Jr, Suguio, K. and Nakamura, T. (2000) The Quaternary geological history of the Santa Catarina southeastern region (Brazil). *An. Acad. Brasil. Cienc.*, 72, 257–270.

Cecil, C. B., Dulong, F. T., Harris, R. A., Cobb, J. C., Gluskoter, H. G., & Nugroho, H. 2003. Observations on climate and sediment discharge in selected tropical rivers, Indonesia. Society for Sedimentary Geology Special Publication No. 77: 29-50.

Cloern J. E., Canuel E. A., Harris D. 2002. Stable carbon and nitrogen isotope composition of aquatic and terrestrial plants of the San Francisco Bay estuarine system. *Limnology and Oceanography* 47:713–729

Collins, A. L., Zhang, Y. S., Duethmann, D., Walling, D. E., and Black, K. S. 2013. Using a novel-trace-tracking framework to source fine-grained sediment loss to watercourses at sub-catchment scale. *Hydrological Processes.* 27(6): 959-974.

Craig, H., and Gordon, L. I. 1965. Deuterium and oxygen 18 variations in the ocean and the marine atmosphere. *Stable Isotopes in Oceanographic Studies and Paleotemperatures.* 9-130.

Cruz, F. W., Karmann, I., Viana, O., Burns, S. J., Ferrari, J. A., Vuille, M., Sial, A. N., and Moreira, M. Z. 2005. Stable isotope study of cave percolation water in subtropical Brazil: Implciations for paleoclimate inferences from spleothems. *Chemical Geology*. 220(3-4): 245-262.

Cruz, F. W. Wang, X., Auler, A., Vuille, M., Burns, S. J., Edwards, L. R. Karmann, I. and Cheng, H. 2009. Orbital and Millennial-Scale Precipitation Changes in Brazil from Speleothem Records. In: F. Vimeux, F. Sylvester, and M. Khodri, editorsPast Climate Variability in South America and Surrounding Regions From the Last Glacial Maximum to the Holocene. Volume 14. Springer. Pp 29-61.

Dansgaard, W. 1964. Stable isotopes in precipitation. *Tellus*. 16(4): 436-468.

Dillenburg, S. R., Tomazelli, L. J., Hesp, P. A., Barboza, E. G., Clerot, L. C. P. and Silva, D. B. 2006. Stratigraphy and evolution of a prograded, transgressive dunefield barrier in southern Brazil. *J. Coastal Res.* 39: 16-20.

Drenzek, N.J., Hughen, K.A., Montluçon, D.B., Southon, J.R., dos Santos, G.M., Druffel, E.R., Giosan, L. and Eglinton, T.I., 2009. A new look at old carbon in active margin sediments. *Geology*, *3*, p.239-242.

Drenzek, N.J., Montluçon, D.B., Yunker, M.B., Macdonald, R.W. and Eglinton, T.I., 2007. Constraints on the origin of sedimentary organic carbon in the Beaufort Sea from coupled molecular 13C and 14C measurements. *Marine chemistry*, *103*(1-2): 146-162.

FitzGerald, D.M., Hein, C. J., Cleary, W., de Menezes, J.T., Klein, A. H. d. F., Scolaro, T., Petsh, S. T., and Buynevich, I. B. 2011. Climatic and sedimentological forcing of strandplain progradation at Tijucas, Central Santa Catarina, Brazil. International Union for Quaternary Research, XVIII INQUA-Congress, 20-27 July, Bern, Switzerland.

FitzGerald, D.M., Hein, C. J., Cleary, W., de Menezes, J.T., Klein, A. H. d. F. 2007. Strandplain evolution along the southern coast of Santa Catarina, Brazil. *J. Coastal Res*. SI50: 152-156.

Farquhar, G. D., O'Leary, M. H. and Berry, J. A. 1982. On the relationship between carbon isotope discrimination and the intercellular carbon dioxide concentration in leaves. *Functional Plant Biology* 9(2): 121-137.

French, K.L., Hein, C.J., Haghipour, N., Wacker, L., Kudrass, H., Eglinton, T.I., Galy, V.V. 2018, Millennial soil retention of terrestrial organic matter deposited in the

Bengal Fan. *Nature Scientific Reports*. v. 8, 11997, doi: 10.1038/s41598-018-30091-8.

Galy, V., Beyssac, O., France-Lanord, C. and Eglinton, T. 2008. Recycling of Graphite During Himalayan Erosion: A Geological Stabilization of Carbon in the Crust. *Science*. 322(5903): 943-945.

Galy, V. and Eglinton, T. 2011. Protracted storage of biospheric carbon in the Ganges-Brahmaputra basin. *Nature Geoscience.* 4: 843-847.

Giannini, P. C. F. 1993. Sistemas Deposicionais no Wuaternario Costeiro entre Jaguaruna e Imbituba, SC. PhD Thesis. Institute of Geosciences, University of Sao Paulo, SP, Brasil.

Hayes, J. M. 2001. Fractionation of Carbon and Hydrogen Isotopes in Biosynthetic Processes. *Reviews in Mineralogy and Geochemistry*. 43(1): 225-277.

Hedges, J.I., Clark, W.A., Quay, P.D., Richey, J.E., Devol, A.H. and Santos, M. 1986. Compositions and fluxes of particulate organic material in the Amazon River1. *Limnology and Oceanography*, *31*(4): 17-738.

Hein, C. J., FitzGerald, D. M., de Menezes, J. T., Cleary, W. J., Klein, A. H. d. F., and Albernaz, M. B. 2014. Sedimentological signatures of the mid-Holocene highstand in Brazil. *Geol. Soc. Am. Bull. 126*: 459-480.

Hein, C. J., FitzGerald, D.M., de Souza, L.H., Georgiou, I.Y., Buynevich, I.V., Klein, A.H.D.F., de Menezes, J.T., Cleary, W.J. and Scolaro, T.L., 2016. Complex coastal change in response to autogenic basin infilling: an example from a sub-tropical Holocene strandplain. *Sedimentology.* 63(6): 1362-1395.

Hilton, R. G., Galy, A., Hovius, N. and Horng, M. J. 2011. Efficient transport of fossil organic carbon to the ocean by steep mountain rivers: an orogenic carbon sequestration mechanism. *Geology.* 39: 71–74.

IAEA/GNIP precipitation sampling guide. 2014. 2(02): 2-20.

IAEA/WMO. 2018. Global Network of Isotopes in Precipitation. The GNIP Database. Accessible at: http://www.iaea.org/water

Instituto Nacional de Meterorólogia, Banco de Dados Meterológicos para Ensino e Pesquisa. Accessible at: http://www.inmet.gov.br/portal/index.php?r=bdmep/bdmep

Isla, F. I. 1989. Holocene sea-level fluctuation in the southern hemisphere. *Quatern. Sci. Rev*. 8: 359-368

Klein, R. M. 1978. Mapa figogeográfico do estado de Santa Catarina. Flora Ilustrada Catarinense.

Klump, J. V. and Martens, C. S. 1981. Biogeochemical cycling in an organic-rich coastal marine basin-II. Nutrient sediment-water exchange processes. Geochim. Cosmochim. Acta. 45:101-121.

Kodama, Y.-M., 1993: Large-scale common features of subtropical convergence zones (the Baiu frontal zone, the SPCZ and the SACZ). Part II: Conditions of the circulations for generating the STCZs. *J. Meteor. Soc. Japan.* 71, 581–610.

Kohn, M. J. 2010. Carbon isotope compositions of terrestrial C3 plants as indicators of (paleo)ecology and (plaeo)climate. *PNAS.* 107(46): 19691-19695.

Kudrass, H. R., Michels, K. R., Wiedicke, M. and Suckow, A. 1998. Cyclones and tides as feeders of a submarine canyon off Bangladesh. *Geology*. 26(8): 715-718.

Kuehl, S. A., Alexander, C. R., Blair, N. E., Harris, C. K., Marsaglia, K. M., Ogston, A. S., Orpin, A. R., Roering, J. J., Bever, A. J., Bilderback, E. L., Carter, L., Cerovski-Darriau, C., Childress, L. B., Corbett, D. R., Hale, R. P., Leithold, E. L., Litchfield, N., Moriarty, J. M., Page, M. J., Pierce, L. E. R., Upton, P. and Walsh, J. P. 2016. A source-to-sink perspective of the Waipaoa River margin. *Earth-Science Reviews*. 153: 301-334.

Ledru, M., Salgado-Labouriau, M. L. and Lorscheitter, M. L. 1998. Vegetation dynamics in southern and central Brazil during the last 10,000 yr BP. Review of Palynology. 99(2):131-142.

Liu, X. and Battisti, D.S. 2015. The influence of orbital forcing of tropical insolation on the climate and isotopic composition of precipitation in South America. *Journal of Climate*. 28: 4842-4862.

Lupker, M., France-Lanord, C., Galy, V., Lave, J. and Kudrass, H. 2013. Increasing chemical weathering in the Himalayan system since the Last Glacial Maximum. *Earth and Planetary Science Letters*. 365: 243-252.

Marengo, J.A., Liebmann, B., Grimm, A. M., Misra, V., Silva Dias, P. L., Calvalcanti, I. F. A., Carvalho, L. M. V., Berbery, E.H., Ambrizzi, T., Vera, C. S., Saulo, A. C., Nogues-Paegle, J., Zipser, E., Seth, A. and Alves, L.M. 2012. Recent developments in the South American monsoon system. *Int. J. Climatol.* 32: 1-21.

Martin, L., Fournier, M., Mourguiart, P., Siefeddine, A. and Turcq, B. 1993. Southern Oscillation signal in South American paleoclimatic data of the last 7000 years. *Quat. Res.* 39: 338-346.

McGlone, M. S., Kershaw, A. P. and Markgraf, V. 1992. El Niño/Southern Oscillation climatic variability in Australasian and South American paleoenvironmental records. In: Diaz, H. F. and Markgraf, V. (Editors). El Niño: Historical and Paleoclimatic Aspects of the Southern Oscillation. Cambridge University Press. Cambridge, pp 435-462.

Milne, G. A., Long, A. J., and Bassett, S. E. 2005. Modeling Holocene relative sea-leve observations from the Caribbean and South America. *Quatern. Sci. Rev*. 24: 1183-1202.

Mitrovica, J. X. and Milne, G. A. 2002. On the origin of late Holocene sea-level highstands within equatorial ocean basins. *Quatern. Sci. Rev*. 21: 24-43.

Nimer, E. 1989. Climatologia do Brasil. IBGE, Departamento de Recursos Naturais e Estudos Ambietais. Rio de Janiero. 421 pp.

Novello, V. F., Cruz, F. W., Moquet, J. S., Vuille, M., de Paula, M. S., Nunes, D., Edwards, R. L., Cheng, H., Karmann, I., Utida, G., Stríkis, N. M. and Campos, J. L. P. S. 2018. Two Millennia of South Atlantic Convergence Zone Variability Reconstructed From Isotopic Proxies. Geophysical Research Letters. 45(10): 5045-5051.

Orselli, J. 1986. Climatologia. Gaplan-SC. Atlas de Santa Catarina. Rio de Janeiro, Brazil. 38-39.

Page, M. J., Trustrum, N. A., Orpin, A. R., Carter, L., Gomez, B., Cochran, U. A., Mildenhall, D. C., Rogers, K. M., Brackley, H. L., Palmer, A. S. and Northcote, L. 2010. Storm frequency and magnitude in response to Holocene climate variability, Lake Tutira, North-Eastern New Zealand. *Marine Geology*. 270(1-4): 30-44.

Pancost, R. D and Boot, C. S. 2004. The paleoclimatic utility of terrestrial biomarkers in marine sediments. *Marine Chemistry.* 92(1-4): 239-261.

Por, F. D. 1992. Sooretama: the Atlantic rain forest of Brazil. SPB, The Hague, 130 pp.

Pruski, A. M. Buscail, R., Bourgeois, S., Vetion, G., Coston-Guarini, J. and Rabouille, C. 2015. Biogeochemistry of fatty acids in a river-dominated Mediterranean ecosystem (Rhone River pro delta, Gulf of Lions, France): Origins and diagenesis. *Organic Geochemistry.* 83-84: 227-240.

Rowe, G. T., Clifford, C. H., Smith, K. L. and Hamilton, P. L. 1975. Benthic nutrient regeneration and its coupling to primary productivity in coastal waters. *Nature.* 255: 215-217.

Roy, P.S., Cowell, P.J., Ferland, M.A. and Thom, B. G. 1994. Wave-dominated coasts. In: Coastal Evolution, Late Quaternary Shoreline Morphodynamics (Eds R. W. G. Carter and C. D. Woodroffe). Cambridge University Press, Cambridge. 121-186.

Schefuß, E., Eglinton, T.I., Spencer-Jones, C.L., Rullkötter, J., De Pol-Holz, R., Talbot, H.M., Grootes, P.M. and Schneider, R.R., 2016. Hydrologic control of carbon cycling and aged carbon discharge in the Congo River basin. *Nature Geoscience*, *9*, p.687.

Schettini, C. A. F., Almeida, D. C., Siegle, E. and Alencar, A. C. B. 2010. A snapshot of suspended sediment and fluid mud occurrence in a mixed-energy embayment, Tijcuas Bay, Brazil. *Geo-Marine Letters.* 30(1): 47-62.

Street-Perrott, F. A., Huang, Y., Perrott, R. A., Eglinton, G., Barker, P., Khelifa, L. B., Harkness, D. D. and Olago, D. O. 1997. Impact of Lower Atmospheric Carbon Dioxide on Tropical Mountain Ecosystems. *Science.* 5342: 1422-1426.

Tamura, T. 2012. Beach ridges and prograded beach deposits as palaeoenvironmental records. *Earth-Science Reviews.* 114: 279-297.

Tamura, T., Nicholas, W.A., Oliver, T. S .N. and Brooke, B. P. 2018. Coarse-sand beach ridges at Cowley Beach, north-eastern Australia: Their formative processes and potential as records of tropical cyclone history. *Sedimentology*. 65: 721-744.

Thornton, S. F. and McManus, J. 1994. Application of Organic Carbon and Nitrogen Stable Isotope and C/N Ratios as Source Indicators of Organic Matter Provenance in Estuarine Systems: Evidence from the Tay Estuary, Scotland. *Estuarine, Coastal and Shelf Science*. 38(3): 219-233.

Tucker, G. E. and Singlerland, R. 1997. Drainage basin responses to climate change. *Water Resources Research: Erosion, Sedimentation and Geomorphology.* 33(8): 2013-2047.

Vuille, M., Burns, S. J., Taylor, B. L., Cruz, F. W., Bird, B. W., Abbott, M. B., Kanner, L. C., Cheng, H. and Novello, V. F. 2012. A review of the South American monsoon history as recorded in stable isotopic proxies over the past two millennia. *Climate of the Past.* 8: 1309-1321.

Wakeham S.G., Canuel E.A. 2006. Degradation and Preservation of Organic Matter in Marine Sediments. In: Volkman J.K. (eds) Marine Organic Matter: Biomarkers, Isotopes and DNA. The Handbook of Environmental Chemistry, vol 2N. Springer, Berlin, Heidelberg

Wang, C., Lee, S. and Enfield, D. B. 2008. Climate Response to Anomously Large and Small Atlantic Warm Pools during the Summer. *Journal of Climate.* 30(4): 2437-2450.

Whipple, K. X. 2009. The influence of climate on the tectonic evolution of mountain belts. *Nature Geoscience.* 2:97-104.

Nardin, W. and Fagherazzi, S. 2018. The role of waves, shelf slope and sediment characteristics on the development of erosional chenier plains. *Geophysical Research Letters.* doi: 10.1029/2018GL078694

Zhou, J. and Lau, K. –M. 1998. Does a monsoon climate exist over South America? *Journal of Climate*. 11:1020-1040.

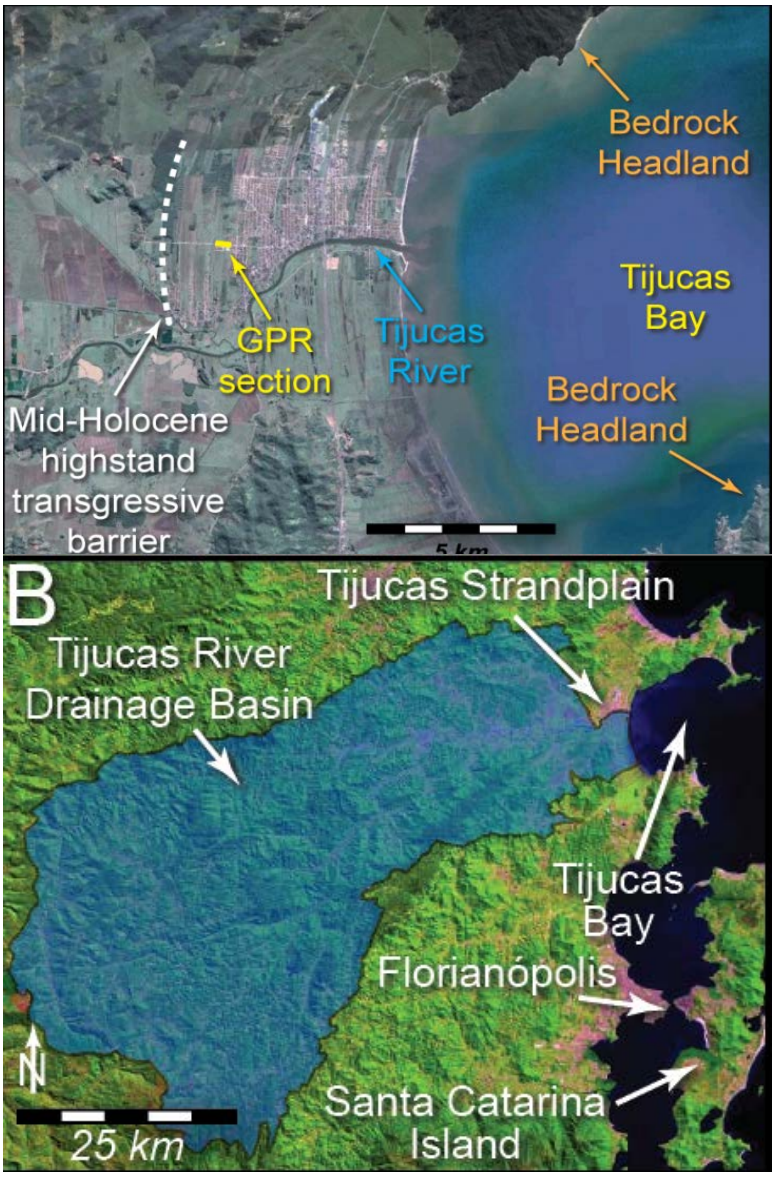

Figure 1. A) Aerial views of the Tijucas River and Strandplain. The landward boundary of the strandplain is marked by a barrier island marking the mid-Holocene highstand, while the modern shoreline fronts the youngest part of the plain. B) Aerial view of the Tijucas River drainage basin. It has a catchment of 2420 km^2 and floodplain of 100 km^2. The river's mean annual discharge is 1.26 km^3 (Schettini *et al.* 2010).

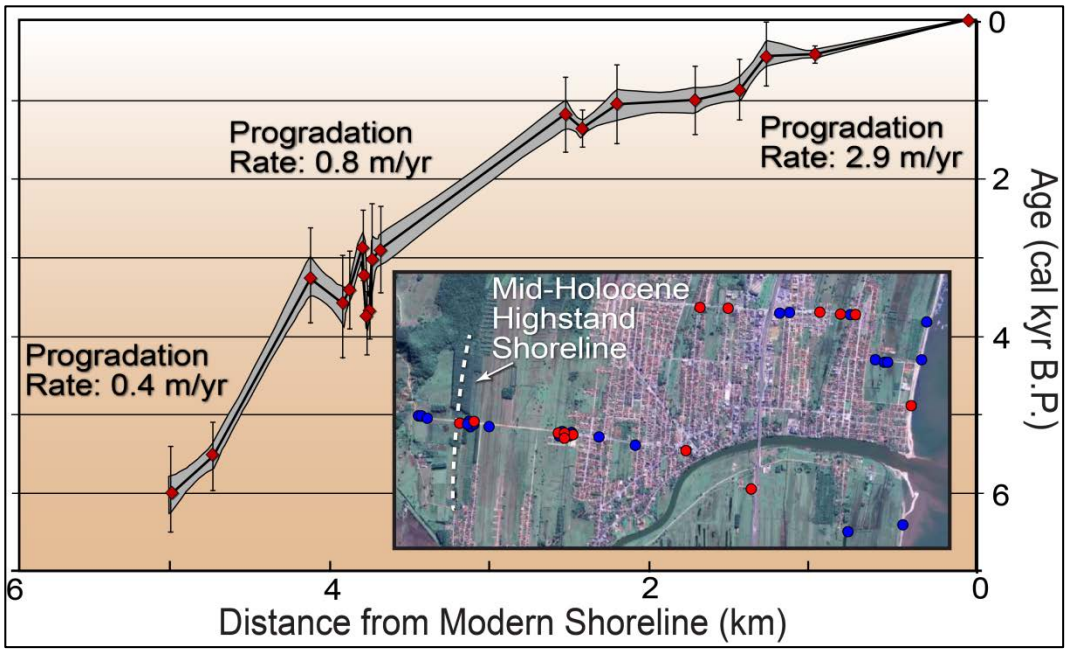

Figure 2. Progradation curve developed via an age-distance model using CLAM 2.1 age-depth modeling software based on 20 calibrated ^{14}C dates collected from various sandy and muddy segments of the Tijucas Strandplain (Hein *et al.* 2016). The blue dots indicate all cores presented by Hein et al. (2016), and the red dots correspond to cores that provided dates for the progradation curve.

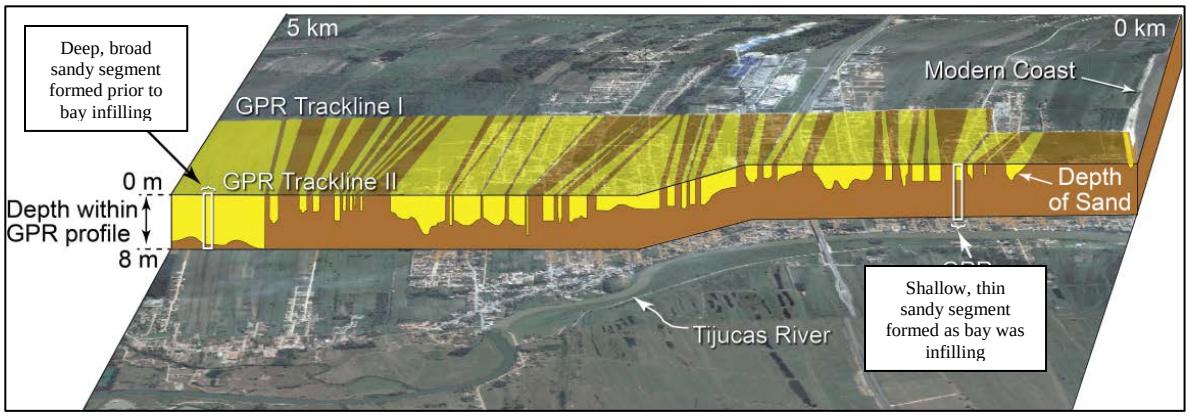

Figure 3. Alternating sections of sandy and muddy strandplain segments distributed across the strandplain as derived from two parallel ground-penetrating radar (GPR) profiles taken across the plain from proximal to the highstand shoreline to the modern shoreline. Yellow sections correspond to sand, while brown sections correspond to mud. The GPR profiles penetrate to *ca.* 8 m below the strandplain surface and depict the general trend of thinning strandplain sediments and reduced sand content in a seaward direction. These observations are consistent with bay infilling with mud over time, as well as the more frequent shifts between sand- and mud- dominated segments. Modified from Hein *et al.* (2016).

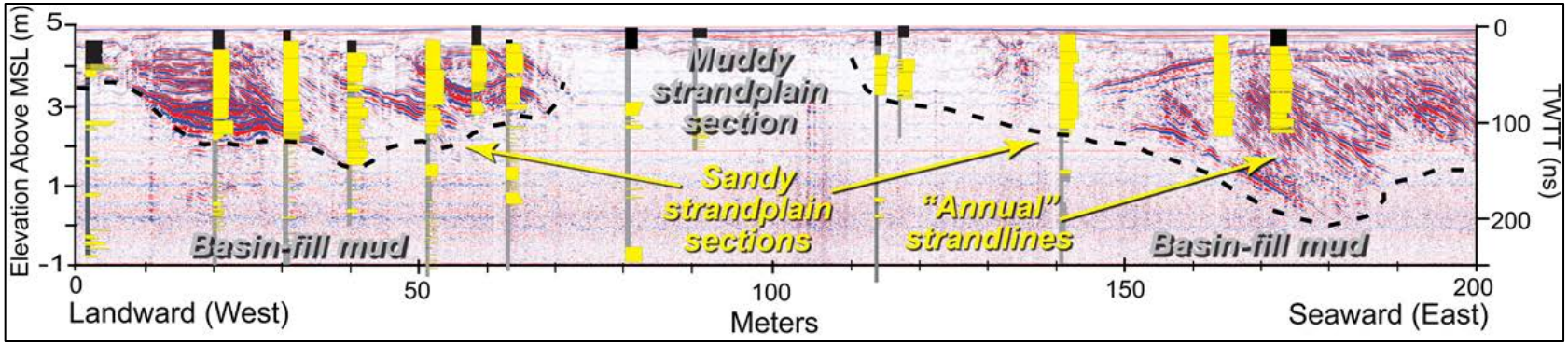

Figure 4. Ground-penetrating radar section depicting a single set of transitions between sandy and muddy sections of the strandplain (C. Hein, unpublished data). White/transparent areas in the GPR section indicate attenuation of radar by mud, while blue and red reflections show subsurface continuations of strandlines (former shorelines) and are generally composed of coarse sand. The thin, gray sections within the graphic core logs are mud, while the thicker yellow sections are sand.

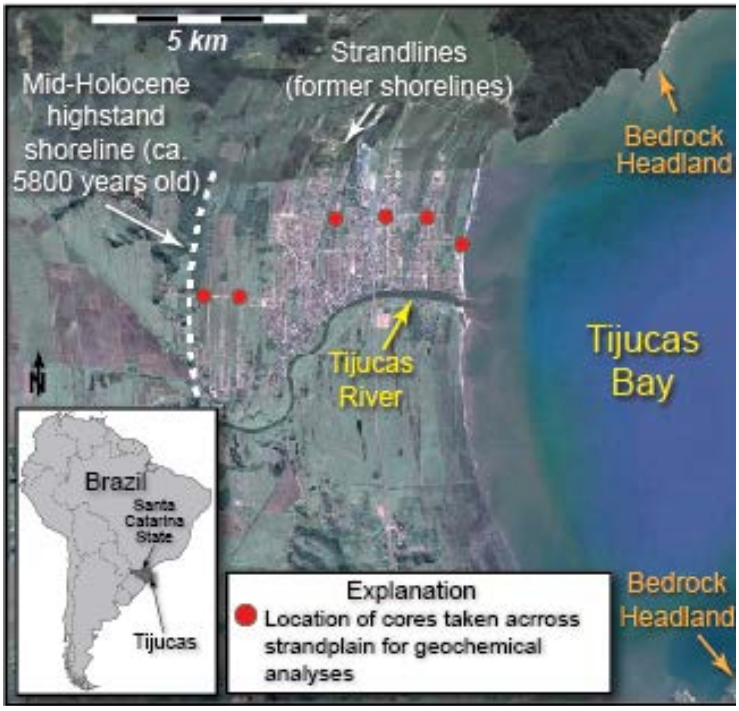

Figure 5a. Aerial view of the Tijucas Strandplain with locations of the six cores collected for geochemical analyses. From the highstand to the modern shoreline, the order of the cores is as follows: TJV-51 (sand), TJV-52 (mud), TJV-56 (sand), TJV-55 (mud), TJV-54 (sand), and TJV-53 (mud).

Figure 5b. Aerial view of the Tijucas River Basin with locations and dates of modern river system samples collected for geochemical analyses. Numbers in parentheses identify "zones" from the river to the beach: upper river (1), middle river (2), lower river (3), estuary (4), and beach/bay (5).

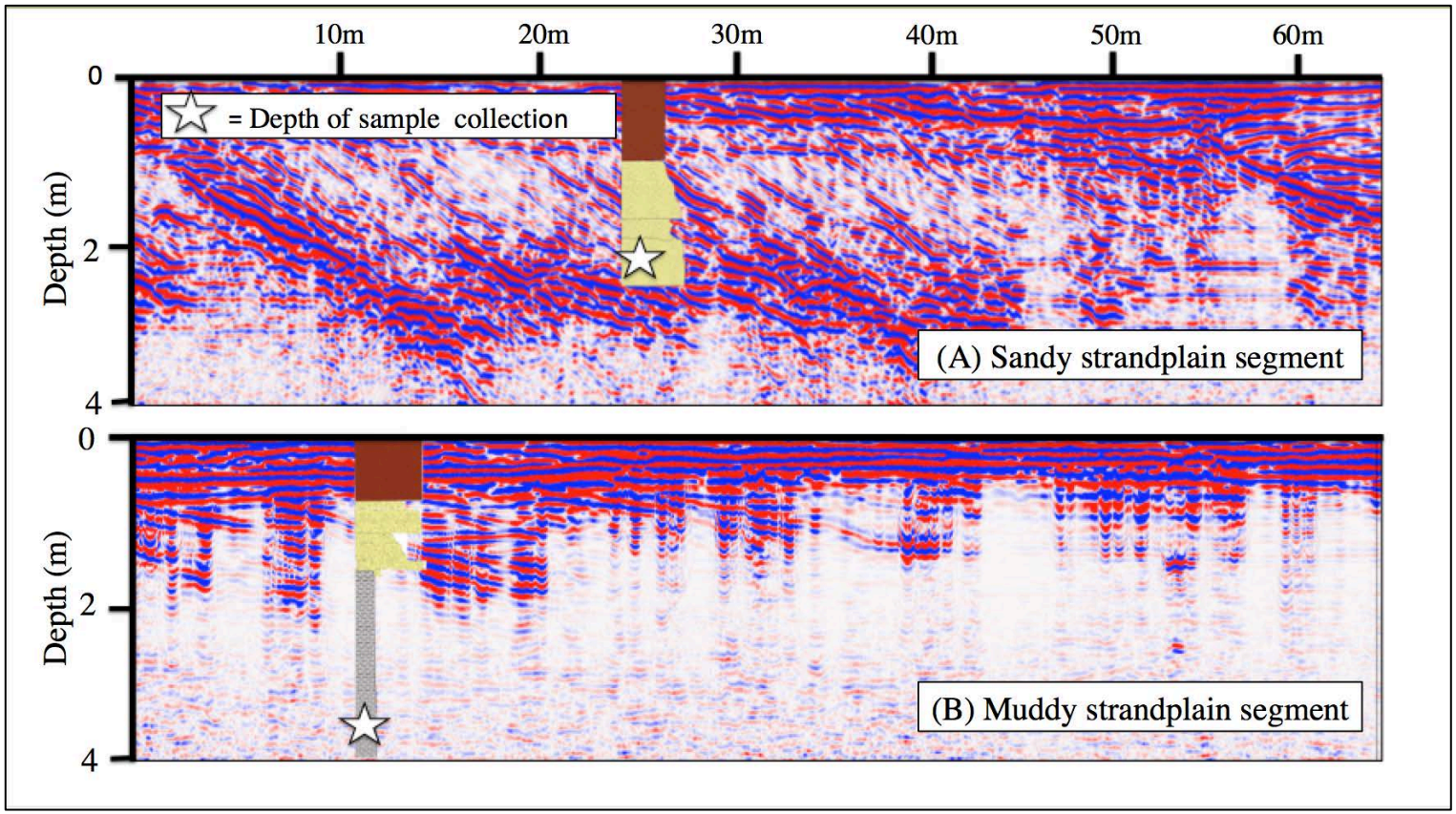

Figure 6. Ground-penetrating radar profiles from representative sandy and muddy segments of the strandplain where cores were collected. Graphic core logs for TJV-56 (A) and TJV-55 (B) depict core stratigraphy and indicate the length of the core as well as the depth of collection of samples for geochemical analysis. Graphic core logs adhere to the standard classification scheme: width of segments in each core log corresponds to sediment texture, where wider units are indicative of coarser sediments, and colors represent interpretation of sediment type: brown corresponds to surficial soil and fill, yellow corresponds to strandplain sands (beach and shoreface), and grey corresponds to strandplain muds (beach, shoreface and basin-fil

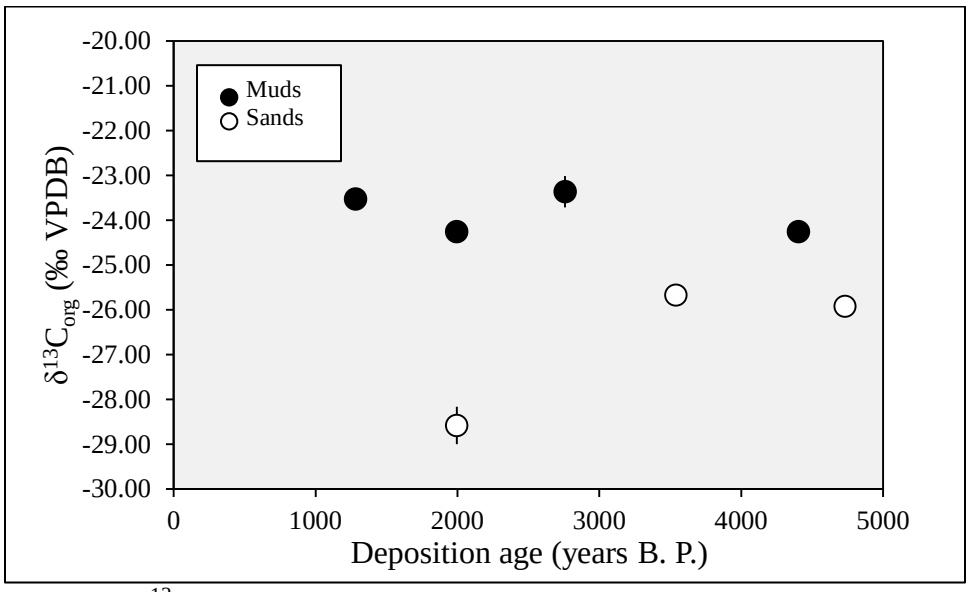

Figure 7. $\delta^{13}C$ values for bulk organic matter in samples collected from cores taken across the strandplain. Age scale is calibrated deposition age in years before present (B.P.), based on interpolation from the strandplain progradation curve of Hein et al. (2016).

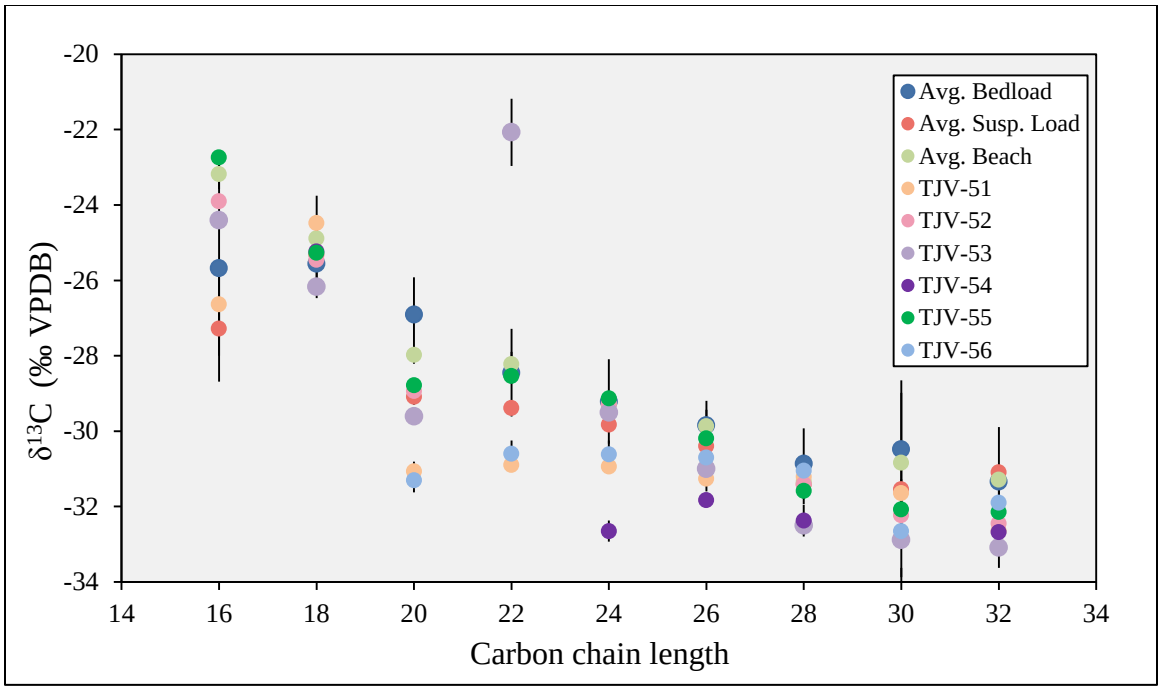

Figure 8. $\delta^{13}C$ values of C_{16}-C_{32} fatty acids from the samples collected from the modern system and cores taken across the strandplain. Bedload samples from 2012, 2015, 2016, 2017 were averaged as well as suspended load samples from 2015 and 2016. The Avg. Beach series represents the average $\delta^{13}C$ values for Tijucas Beach 2015 and 2017 and Tijucas Bay 2016 samples.

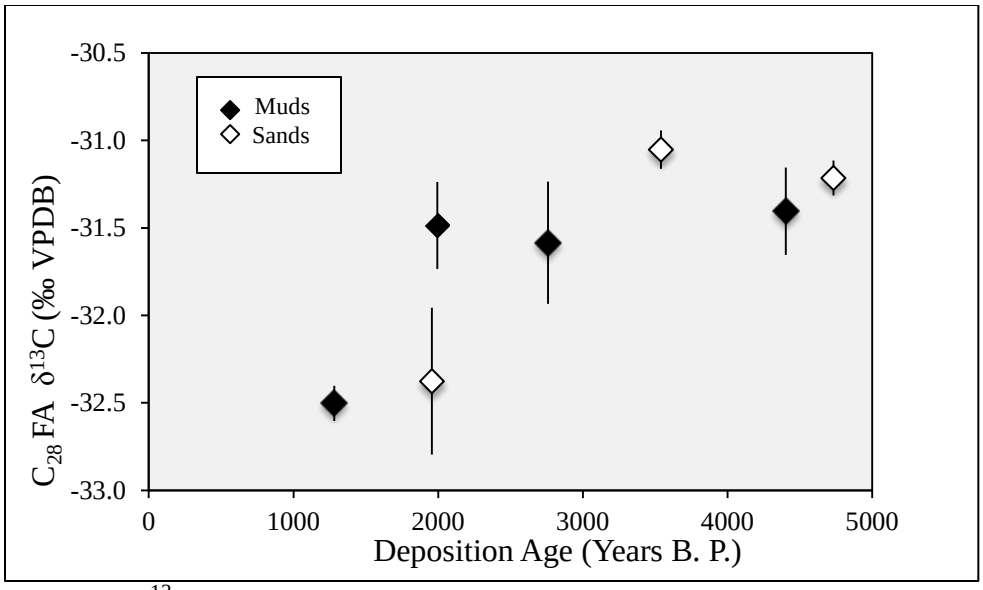

Figure 9. $\delta^{13}C$ values of C_{28} fatty acids in sediments collected from cores taken across the strandplain. Age scale is calibrated deposition age in years before present (B.P.), based on interpolation from the strandplain progradation curve of Hein et al. (2016).

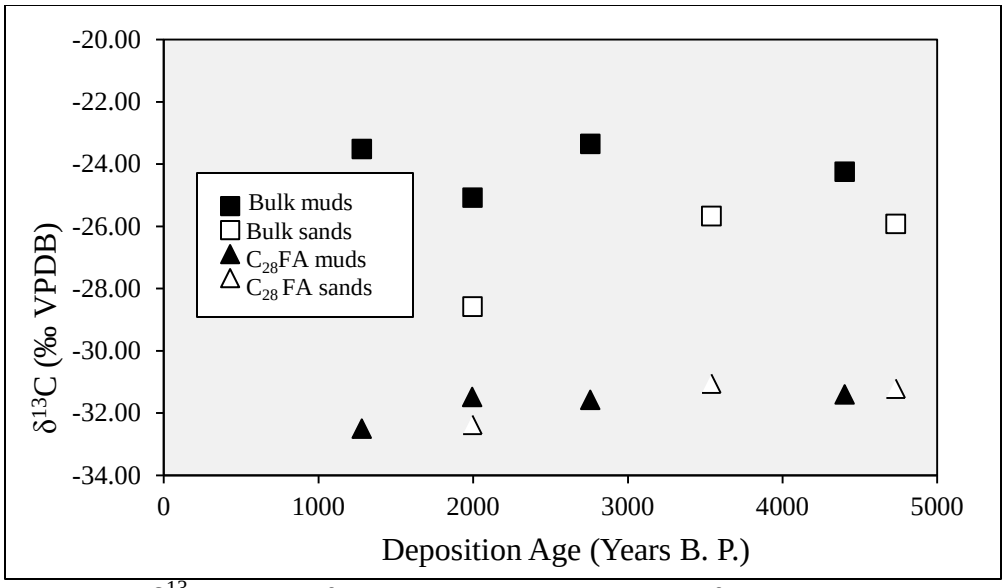

Figure 10. $\delta^{13}C$ values of bulk organic carbon and C_{28} fatty acids in sediments collected from cores taken across the Tijucas Strandplain (see Figure 5b for locations). Age scale is calibrated deposition age in years before present (B.P.), based on interpolation from the strandplain progradation curve of Hein et al. (2016).

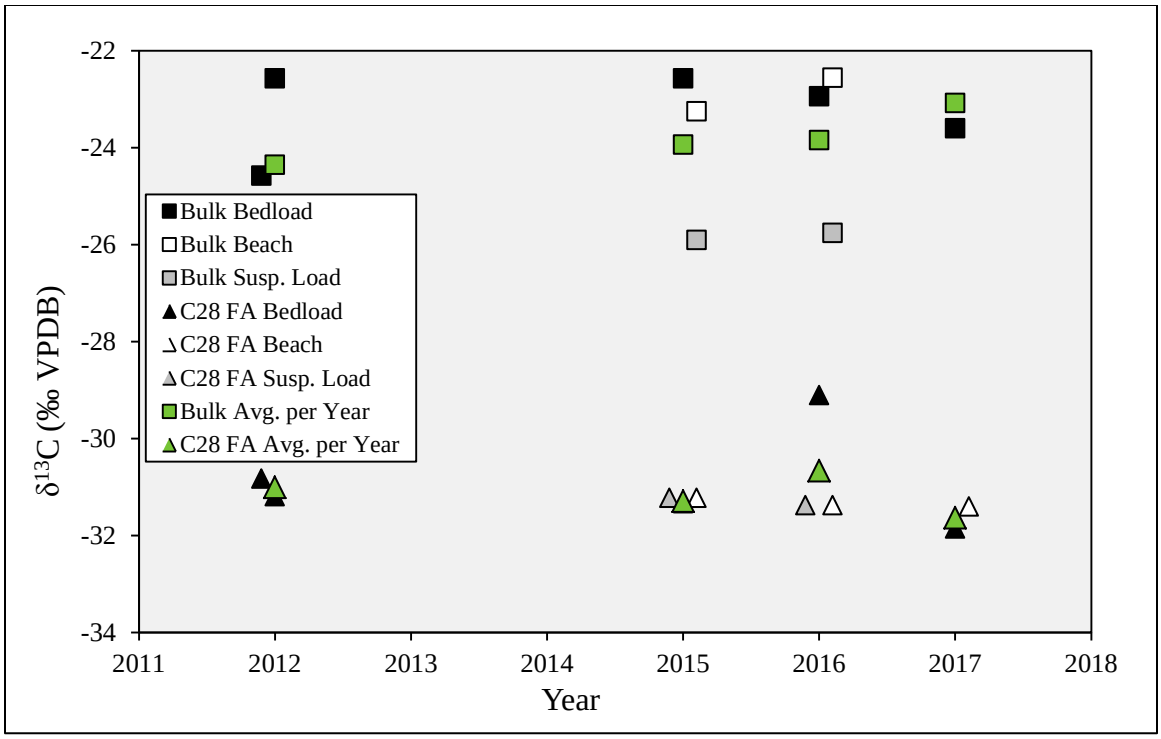

Figure 11. $\delta^{13}C$ values of samples collected from the modern river system from years 2012, 2015, 2016 and 2017 as well as the average $\delta^{13}C$ value for all modern samples from each particular year (green symbols). The Tijucas Bay sample was considered to be a "beach" sample from 2016 for simplification.

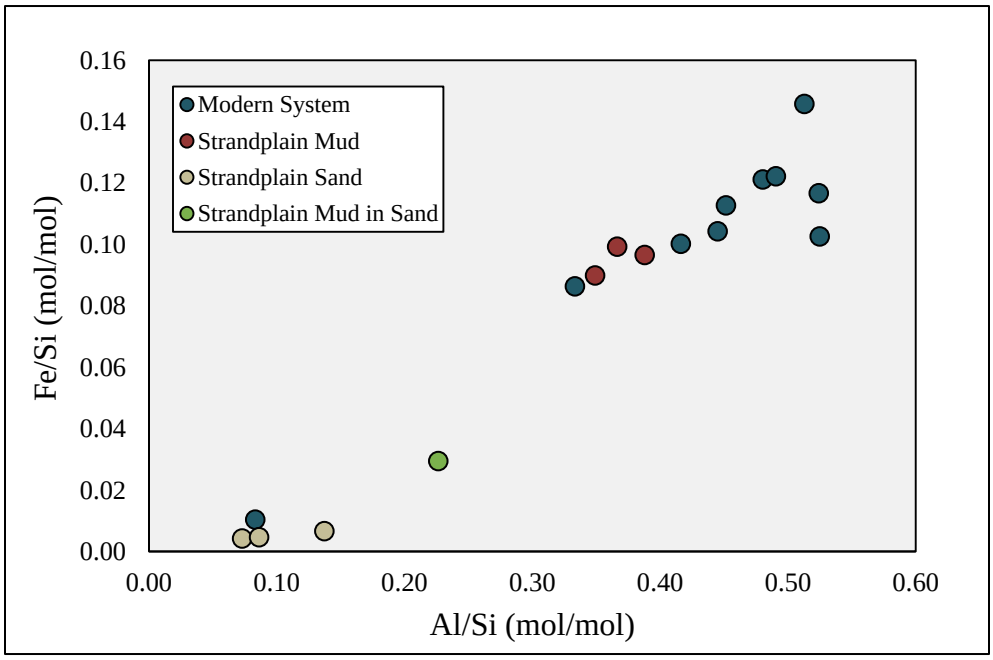

Figure 12. Fe/Si ratio, a proxy for weathering, as a function of Al/Si ratio, a proxy for grain size, for all modern system and strandplain samples, distinguished by sample location and sediment type.

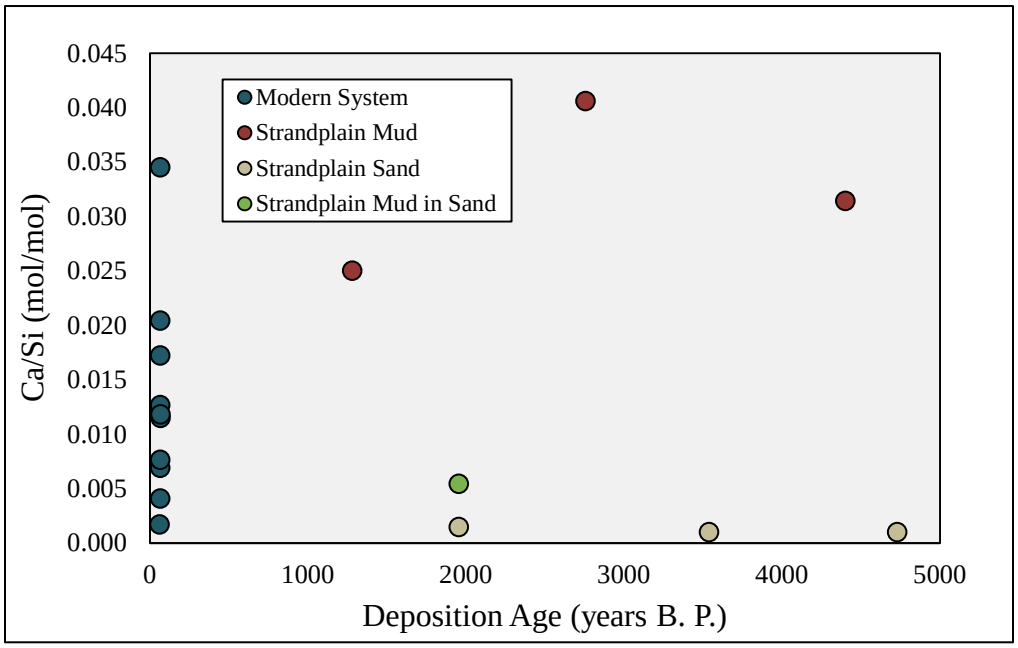

Figure 13. Temporal proxy record of weathering based on Ca/Si ratios as a function of deposition age. Modern system Ca/Si ratios are considered to have a deposition age of 0. Nearly all strandplain samples plot within variability of the modern system, with strandplain mud more chemically weathered than sands (and relatively coarse mud co-deposited with sand).

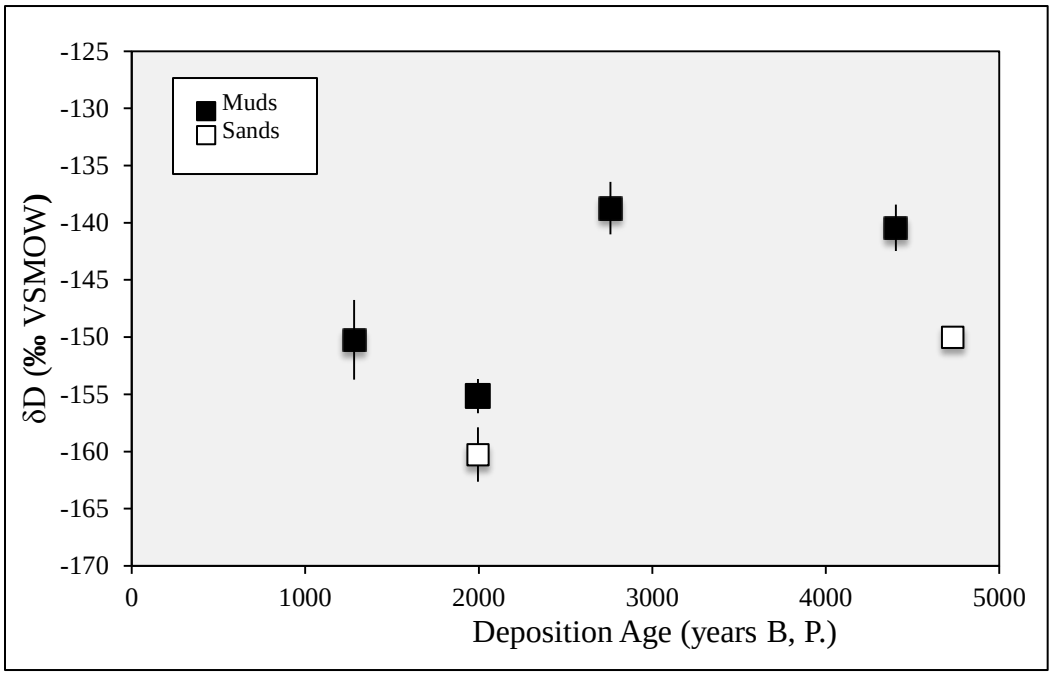

Figure 14. δD values for C_{28} fatty acids in sediments collected from cores taken across the strandplain. Age scale is calibrated deposition age in years before present (B.P.), based on interpolation from the strandplain progradation curve of Hein et al. (2016).

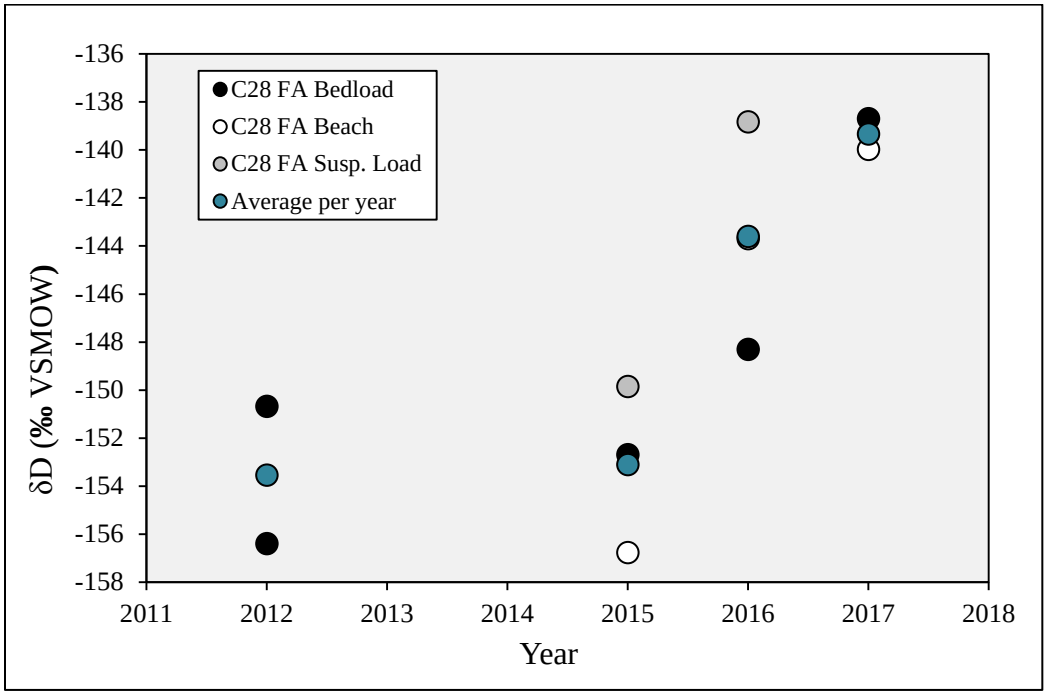

Figure 15. Stable-hydrogen isotopic composition of Tijucas Beach, Tijucas Bay and Tijucas Bedload samples collected from the modern system over the years 2012, 2015, 2016 and 2017. The δD values for C_{28} fatty acids as well as the sample averages by year. The Tijucas Bay sample was considered to be a "beach" sample from 2016 for simplification.

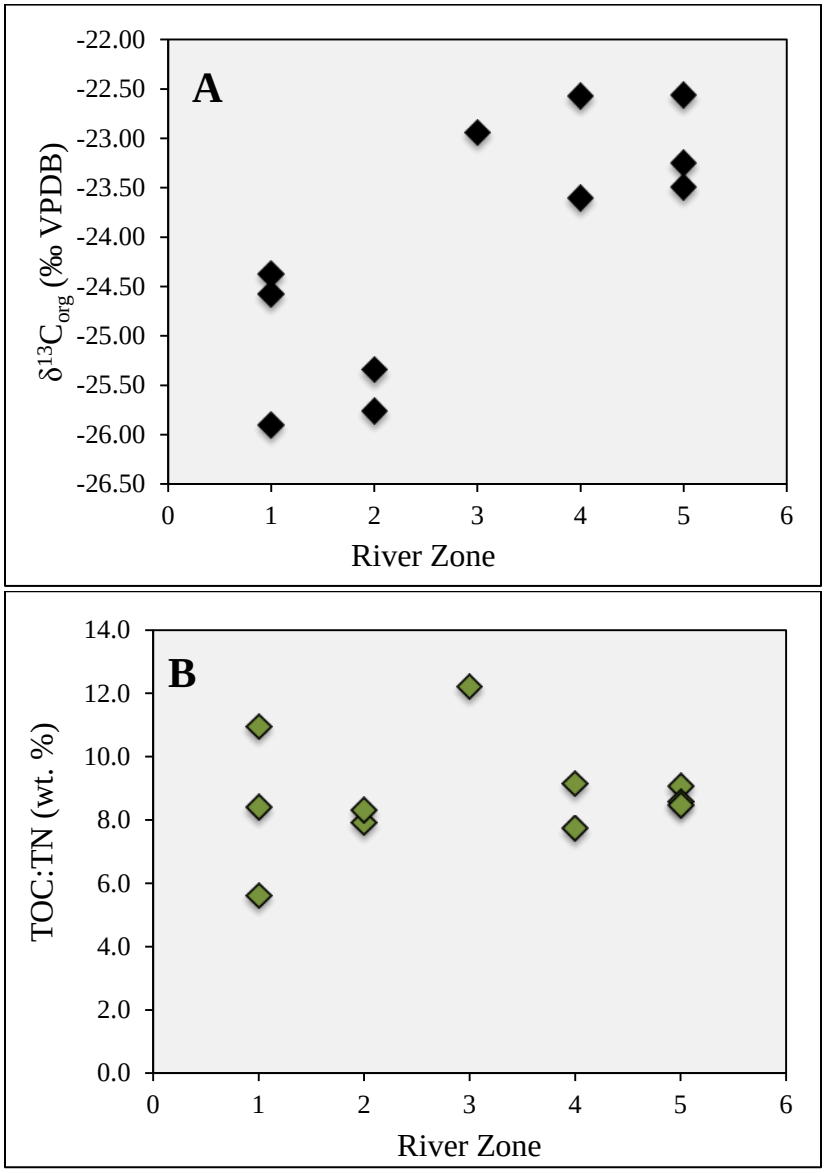

Figure 16. Bulk $\delta^{13}C$ (A) and TOC:TN (B) values for all modern system samples subdivided by "river zone" (see Figure 5b). Zone 1 refers to the most inland sampling location on the Tijucas River and zone 5 refers to the estuarine-most sampling zone. All zones and samples collected from each are indicated on Figure 2.

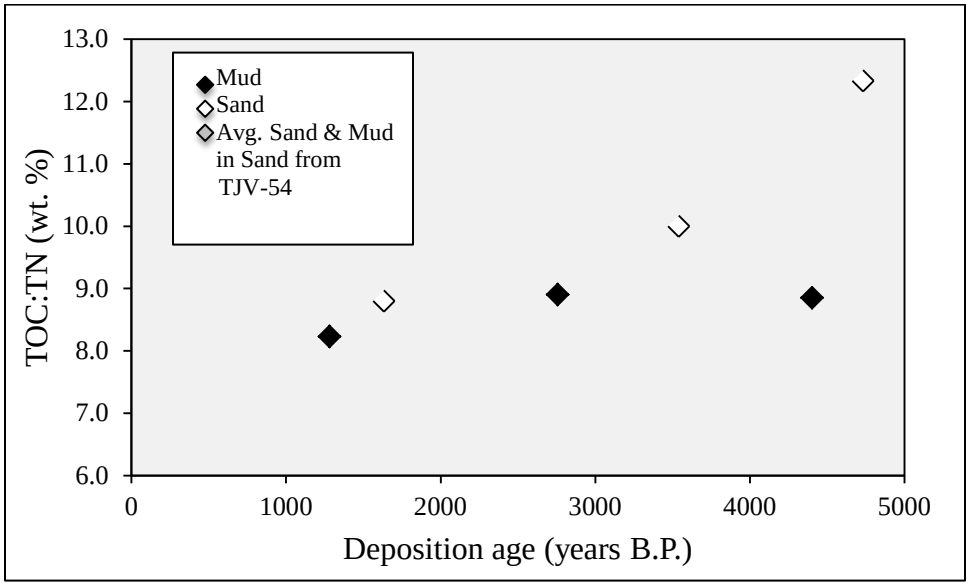

Figure 17. TOC: TN values for sediment samples collected across the strandplain.

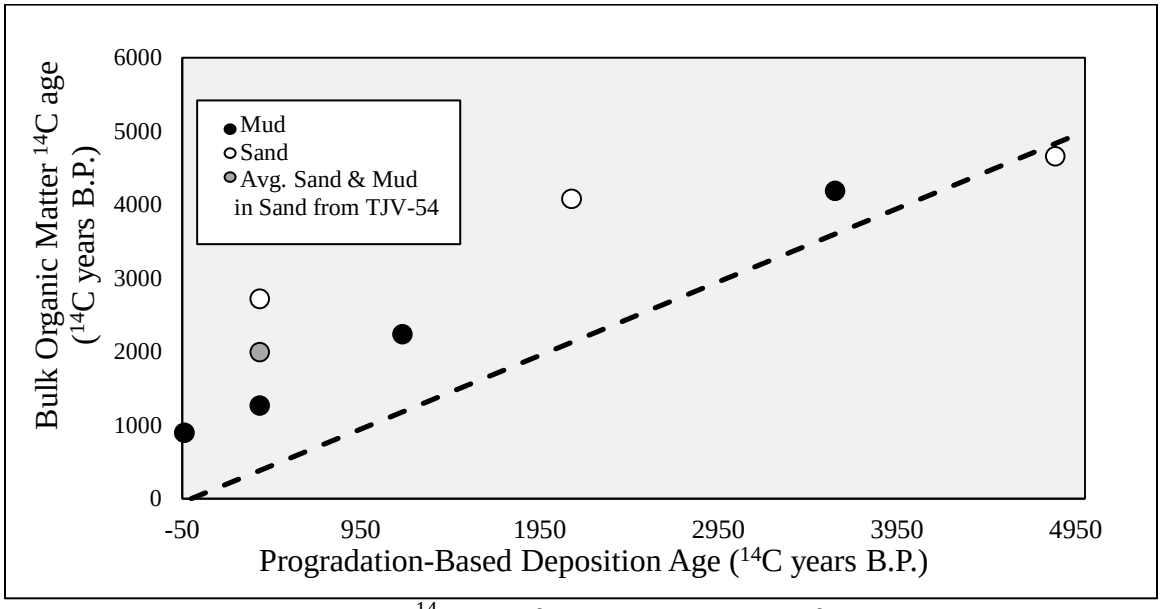

Figure 18. Bulk organic matter ^{14}C ages for samples collected from the strandplain depicted as a function of deposition age, also given in ^{14}C years. Values plotting above the 1:1 line indicate pre-aging of organic matter (i.e., addition of old, likely soil-derived, organic matter) to the overall organic matter pool prior to deposition in the strandplain.

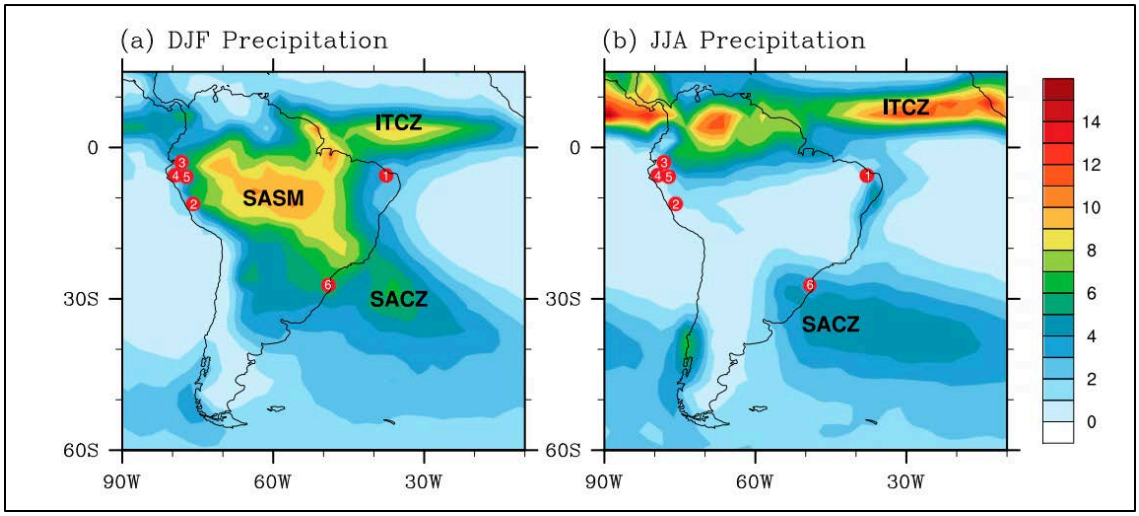

Figure 19. Modified from Liu and Battisti 2015. Depiction of (A) South American Summer Monsoon precipitation pattern during austral summer and (B) precipitation patterns associated with the South Atlantic Convergence Zone during austral winter. The white star indicates the approximate location of Tijucas.

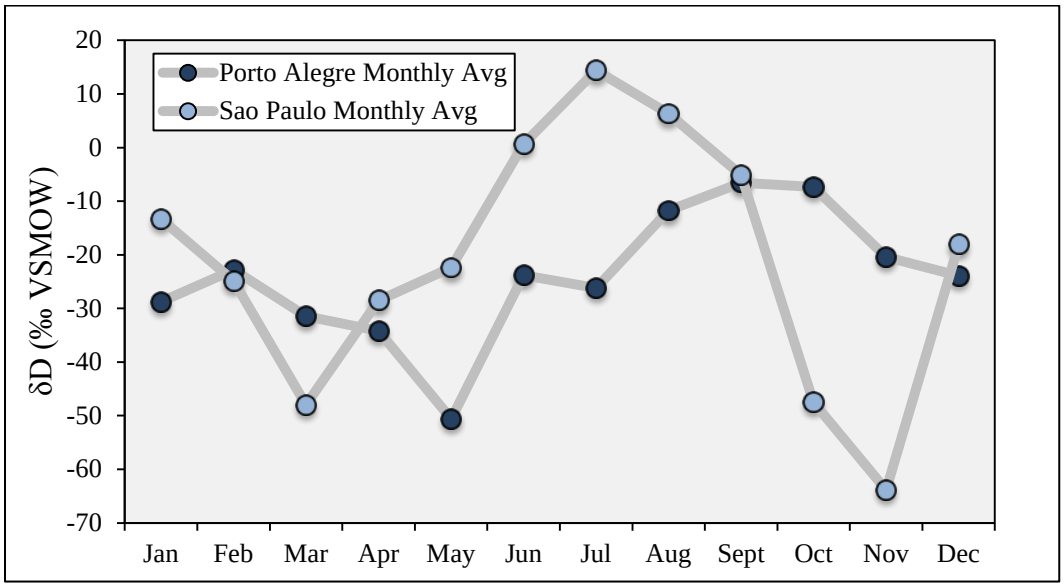

Figure 20. Average monthly δD values of precipitation from 2013 and 2014 at Rio Clara in São Paulo State, southern Brazil and from 1976-1979 at Porto Alegre in the state of Rio Grande do Sul, southern Brazil.

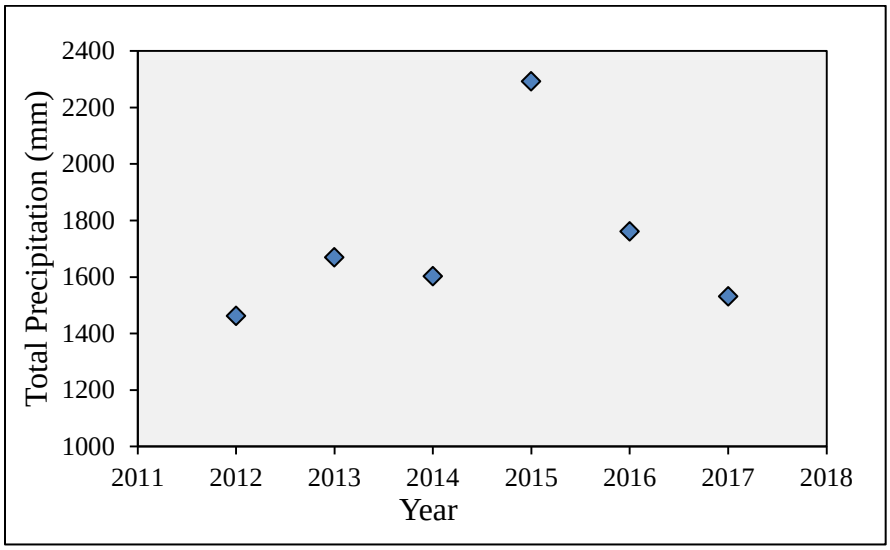

Figure 21. Total annual precipitation volume from 2012-2017 based on monthly measurements at Florianópolis, Santa Catarina State, southern Brazil (Instituto Nacional de Meterorólogia 2018).

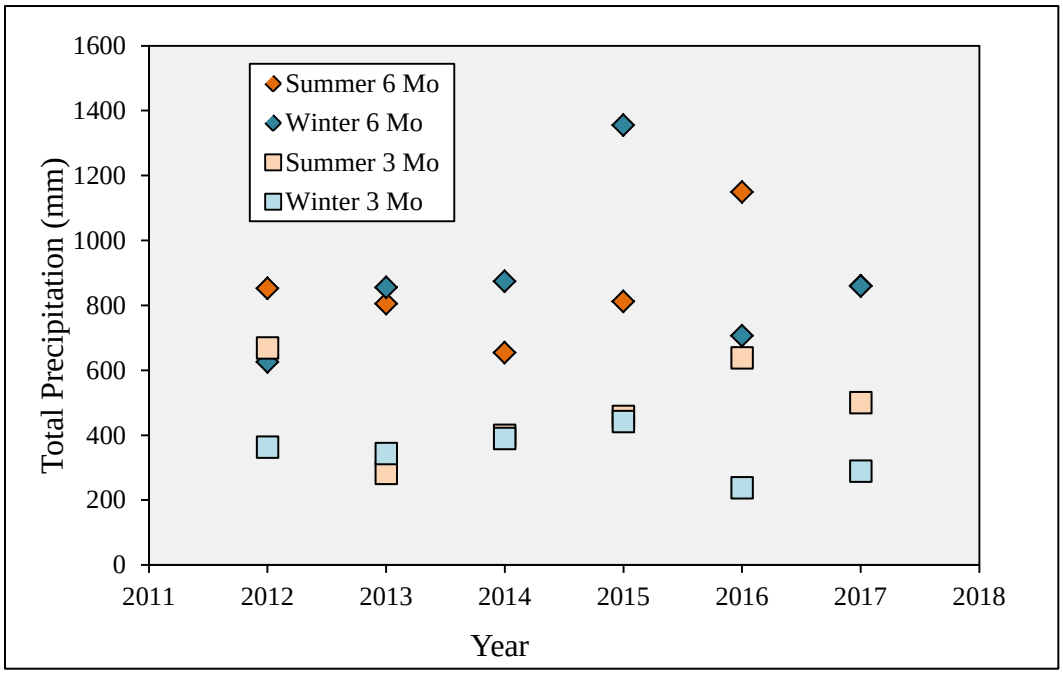

Figure 22. Total precipitation amount from 2012-2017 based on monthly measurements at Florianópolis, Santa Catarina State, southern Brazil, subdivided into 3-month austral summer (Nov, Dec, Jan) and austral winter (Jun, Jul, Aug) periods as well as 6-month austral summer (Nov-Mar) and austral winter (Apr-Oct) periods. Note large spike in rainfall during winter 2015 (concentrated in the Sept to Oct time period), during the period preceding the April 2016 sampling period.

Core	Latitude	Longitude	Ridge/sample type	Sampling Depth within Core	Total Core Depth	Depo. Age (years B.P.)
TJV-51	27°14'30.45"S	48°39'43.40"W	Sandy	192-232 cm	398 cm	4131
TJV-52	27°14'32.48"S	48°39'27.11"W	Muddy	350-362 cm	586 cm	4402
TJV-53	27°14'09.54"S	48°36'56.91"W	Muddy	305-315 cm	590 cm	1281
TJV-54	27°13'50.82"S	48°37'24.86"W	Sandy	188-213 cm	322 cm	1956
TJV-55	27°13'50.18"S	48°38'05.68"W	Muddy	220-230 cm	233 cm	2758
TJV-56	27°13'46.08"S	48°38'42.22"W	Sandy	154-174 cm	230 cm	3539
Mud in sand	27°13'50.82"S	48°37'24.86"W	Sandy	230-316 cm	316 cm	1956

Table 1. Core locations across the Tijucas Strandplain and the associated ridge type (sandy strandplain section or muddy strandplain section), as well as total core depth and the depth below the ground surface from which associated sand or mud samples were collected for geochemical analysis.

Table 2. Sample type, date collected and location of sediments collected from the modern river, estuarine and beach environments over the years 2012, 2015, 2016, and 2017.

Sample	Date collected	Latitude	Longitude
Bedload sand	April 2012	27°16'13.03"S	48°41'46.38"W
Bedload mud	April 2012	27°16'14.80"S	48°41'47.36"W
Suspended load	April 2012	27°16'14.80"S	48°41'47.36"W
Beach mud	April 2015	27°14'34.65"S	48°36'49.15"W
Bedload mud	April 2015	27°15'23.33"S	48°38'51.64"W
Suspended load	April 2015	27°15'45.47"S	48°39'49.93"W
Bay mud	April 2016	27°14'32.17"S	48°36'34.78"W
Floodplain mud	April 2016	27°15'54.76"S	48°39'20.70"W
Bedload mud	April 2016	27°15'53.78"S	48°39'18.90"W
Suspended load	April 2016	27°15'45.47"S	48°39'49.93"W
Beach mud	April 2017	27°14'34.65"S	48°36'49.15"W
Bedload mud	April 2017	27°15'23.33"S	48°38'51.64"W

Sample ID	TOC:TN
Tijucas Suspended Load 2012	5.6
Tijucas Bedload Sand 2012	8.4
Tijucas Bedload Mud 2012	11.0
Tijucas River Bedload Mud 2015	7.7
Tijucas River Suspended Load 2015	7.9
Tijucas Beach 2015	9.1
Tijucas River Bedload Mud 2016	12.2
Tijucas River Suspended Load 2016	8.3
Tijucas River Floodplain 2016	11.7
Tijucas Bay Mud 2016	8.6
Tijucas Beach 2017	8.5
Tijucas River Bedload Mud 2017	9.2
TJV-51 (sand)	12.3
TJV-52 (mud)	8.8
TJV-53 (mud)	8.2
TJV-54 (sand)	8.8
TJV-55 (mud)	8.9
TJV-56 (sand)	10.0
TJV-54 (mud within sand)	11.1

Table 3. Total organic carbon to total nitrogen ratios for all samples.

Sample ID	F Modern	FM Error	Latitude	Longitude	NOSAMS Accession Number	$\delta^{13}C$ (‰)	Reported age (yrs BP)	Reported age error	$\Delta^{14}C$
Tijucas Suspended Load 2012	0.7333	0.0038	27°16'14.80"S	48°41'47.36"W	52524.1.1*	-38-30	2,492	42	-272.3
Tijucas Bedload Sand 2012	0.6864	0.0023	27°16'13.03"S	48°41'46.38"W	OS-127760	-25.78	3020	25	-318.8
Tijucas Bedload Mud 2012	0.6083	0.0041	27°16'14.80"S	48°41'47.36"W	52523.1.1*	-24.70	3,992	54	-396.3
Tijucas River Bedload Mud 2015	0.9300	0.0031	27°15'23.33"S	48°38'51.64"W	OS-135110	-22.78	585	20	-77.3
Tijucas River Suspended Load 2015	0.7623	0.0022	27°15'45.47"S	48°39'49.93"W	OS-135364	-26.04	2180	25	-243.7
Tijucas Beach 2015	0.9042	0.0029	27°14'34.65"S	48°36'49.15"W	OS-135260	-23.75	810	25	-102.9
Tijucas River Bedload Mud 2016	0.4678	0.0031	27°15'53.78"S	48°39'18.90"W	OS-135111	-20.57	6100	55	-535.9
Tijucas River Suspended Load 2016	0.8812	0.0019	27°15'45.47"S	48°39'49.93"W	OS-135259	-25.57	1020	15	-125.8
Tijucas River Floodplain 2016	0.9418	0.0020	27°15'54.76"S	48°39'20.70"W	OS-135365	-24.08	480	15	-65.7
Tijucas Bay Mud 2016	0.8995	0.0019	27°14'32.17"S	48°36'34.78"W	OS-135262	-23.08	850	20	-107.6
Tijucas Beach 2017	0.9331	0.0019	27°14'34.65"S	48°36'49.15"W	OS-135261	-22.73	555	15	-74.4
Tijucas River Bedload Mud 2017	0.9111	0.0022	27°15'23.33"S	48°38'51.64"W	OS-135112	-23.57	750	20	-96.3
TJV-51 (sand)	0.5596	0.0016	27°14'30.45"S	48°39'43.40"W	OS-135150	-25.91	4660	25	-444.8
TJV-52 (mud)	0.6020	0.0016	27°14'32.48"S	48°39'27.11"W	OS-135107	-22.15	4080	20	-402.7
TJV-53 (mud)	0.8940	0.0019	27°14'9.54"S	48°36'56.91"W	OS-135108	-21.93	900	15	-113.0
TJV-54 (sand)	0.7131	0.0017	27°13'50.82"S	48°37'24.86"W	OS-135697	-21.48	2720	20	-276.1
TJV-55 (mud)	0.7571	0.0023	27°13'50.18"S	48°38'5.68"W	OS-135109	-30.35	2240	15	-248.8
TJV-56 (sand)	0.5935	0.0017	27°13'46.08"S	48°38'42.22"W	OS-135152	-25.67	4190	25	-411.2
TJV-54 (mud within sand)	0.8538	0.0019	27°13'50.82"S	48°37'24.86"W	OS-135367	-23.86	1270	20	-153.1

Table 4. Bulk radiocarbon measurements for all samples, reported with location and NOSAMS Accession Number. Measurements are reported in fraction modern (between 0 and 1), ^{14}C years B. P. and $\Delta^{14}C$. For samples with accession numbers denoted with an asterisk (*), radiocarbon analyses were conducted at ETH Zurich and the listed number refers to this institution as opposed to NOSAMS.

Sample ID	Bulk OM $\delta^{13}C$ (‰)
Tijucas Suspended Load 2012	-25.90
Tijucas Bedload Sand 2012	-24.58
Tijucas Bedload Mud 2012	-24.38
Tijucas River Bedload Mud 2015	-22.57
Tijucas River Suspended Load 2015	-25.76
Tijucas Beach 2015	-23.49
Tijucas River Bedload Mud 2016	-22.94
Tijucas River Suspended Load 2016	-25.34
Tijucas River Floodplain 2016	-24.22
Tijucas Bay Mud 2016	-23.25
Tijucas Beach 2017	-22.56
Tijucas River Bedload Mud 2017	-23.60
TJV-51 (sand)	-25.92
TJV-52 (mud)	-24.25
TJV-53 (mud)	-23.52
TJV-54 (sand)	-28.58
TJV-55 (mud)	-23.36
TJV-56 (sand)	-25.67
TJV-54 (mud within sand)	-24.25

Table 5. $\delta^{13}C$ bulk organic matter isotopic compositions for all samples.

Sample ID	C_{24}(‰)	C_{26}(‰)	C_{28} (‰)	C_{30}(‰)	C_{32}(‰)
Tijucas Bedload Sand 2012	-30.63	-30.67	-30.86	-31.84	-32.48
Tijucas Bedload Mud 2012	-29.81	-30.07	-31.20	-31.96	-32.87
Tijucas River Bedload Mud 2015	-28.84	-29.61	-31.33	-27.71	-31.00
Tijucas River Suspended Load 2015	-29.94	-30.36	-31.31	-31.49	-31.04
Tijucas Beach 2015	-29.65	-30.05	-31.23	-28.69	-31.20
Tijucas River Bedload Mud 2016	-27.27	-28.72	-29.10	-28.86	-28.81
Tijucas River Suspended Load 2016	-29.72	-30.44	-31.52	-31.60	-31.14
Tijucas River Floodplain 2016	-29.30	-19.76	-32.07	-31.96	-31.78
Tijucas Bay Mud 2016	-29.06	-29.37	-31.37	-31.97	-31.73
Tijucas Beach 2017	-29.11	-30.18	-31.40	-31.85	-30.93
Tijucas River Bedload Mud 2017	-29.64	-30.27	-31.86	-32.01	-31.45
TJV-51 (sand)	-30.94	-31.26	-31.21	-31.64	-32.64
TJV-52 (mud)	-29.29	-18.70	-31.40	-32.23	-32.45
TJV-53 (mud)	-29.50	-31.00	-32.50	-32.88	-33.08
TJV-54 (sand)	-32.65	-31.83	-32.38	-34.07	-32.68
TJV-55 (mud)	-29.13	-30.19	-31.58	-32.08	-32.14
TJV-56 (sand)	-30.62	-30.70	-31.05	-32.65	-31.90
TJV-54 (mud within sand)	-29.58	-30.01	-31.49	-31.73	-30.57

Table 6. $\delta^{13}C$ isotopic compositions for all samples of C_{24}-C_{32} long chain fatty acids.

Sample ID	Year/ID	Al/Si (mol/mol)	Fe/S (mol/mol)	Ca/Si (mol/mol)
Tijucas River Suspended Load	April 2015	0.51	0.1457	0.0069
Tijucas River Suspended Load	April 2016	0.52	0.1167	0.0077
Tijucas River Bedload Sand	April 2012	0.083	0.0104	0.0017
Tijucas River Bedload Mud	April 2015	0.48	0.1212	0.0127
Tijucas River Bedload Mud	April 2016	0.33	0.0863	0.0345
Tijucas River Bedload Mud	April 2017	0.49	0.1221	0.0115
Tijucas River Floodplain	April 2016	0.52	0.1027	0.0041
Tijucas Bay	April 2016	0.42	0.1002	0.0172
Tijucas Beach	April 2015	0.45	0.1127	0.0204
Tijucas Beach	April 2017	0.44	0.1043	0.0118
TJV-51	Sand	0.073	0.0042	0.0010
TJV-52	Mud	0.35	0.0899	0.0314
TJV-53	Mud	0.39	0.0966	0.0250
TJV-54	Sand	0.14	0.0067	0.0015
TJV-54	Mud in Sand	0.23	0.0295	0.0055
TJV-55	Mud	0.37	0.0993	0.0406
TJV-56	Sand	0.09	0.0047	0.0010

Table 7. Al/Si, Fe/Si and Ca/Si values for all samples.

Sample ID	C28 (‰)	C30(‰)	C32(‰)
Tijucas Bedload Sand 2012	-156.39	-152.48	-147.43
Tijucas Bedload Mud 2012	-150.68	-154.01	-143.03
Tijucas River Bedload Mud 2015	-152.69	-150.24	-156.27
Tijucas River Suspended Load 2015	-149.85	-145.90	-144.83
Tijucas Beach 2015	-156.77	-149.99	-149.64
Tijucas River Bedload Mud 2016	-148.30	-149.76	-150.75
Tijucas River Suspended Load 2016	-138.83	-141.02	N/A
Tijucas River Floodplain 2016	-151.70	-145.00	-143.50
Tijucas Bay Mud 2016	-143.69	-140.46	-138.53
Tijucas Beach 2017	-139.98	-136.95	-132.54
Tijucas River Bedload Mud 2017	-138.69	-135.42	-133.85
TJV-51 (sand)	-150.00	-146.10	N/A
TJV-52 (mud)	-140.45	-134.35	-133.40
TJV-53 (mud)	-150.24	-145.97	-145.27
TJV-54 (sand)	-160.27	-132.76	-140.93
TJV-55 (mud)	-138.72	-131.71	-133.54
TJV-56 (sand)	N/A	N/A	N/A
TJV-54 (mud within sand)	-155.16	-146.10	-148.18

Table 8. δD isotopic compositions for all samples for C_{28}-C_{32} long chain fatty acids.